

Visual cortical networks for “What” and “Where” to the human hippocampus revealed with dynamical graphs

Edmund T. Rolls^{1,2,3,*} and Tatyana S. Turova⁴

¹Oxford Centre for Computational Neuroscience, Oxford, United Kingdom

²Department of Computer Science, University of Warwick, Coventry CV4 7AL, United Kingdom

³Institute for the Science and Technology of Brain Inspired Intelligence, Fudan University, China

⁴Mathematical Center, University of Lund, 22100 Lund, Sweden

*Corresponding author: Edmund T. Rolls, Department of Computer Science, University of Warwick, Coventry CV4 7AL, United Kingdom.

Email: Edmund.Rolls@oxcns.org

Key questions for understanding hippocampal function in memory and navigation in humans are the type and source of visual information that reaches the human hippocampus. We measured bidirectional pairwise effective connectivity with functional magnetic resonance imaging between 360 cortical regions while 956 Human Connectome Project participants viewed scenes, faces, tools, or body parts. We developed a method using deterministic dynamical graphs to define whole cortical networks and the flow in both directions between their cortical regions over timesteps after signal is applied to V1. We revealed that a ventromedial cortical visual “Where” network from V1 via the retrosplenial and medial parahippocampal scene areas reaches the hippocampus when scenes are viewed. A ventrolateral “What” visual cortical network reaches the hippocampus from V1 via V2–V4, the fusiform face cortex, and lateral parahippocampal region TF when faces/objects are viewed. There are major implications for understanding the computations of the human vs rodent hippocampus in memory and navigation: primates with their fovea and highly developed cortical visual processing networks process information about the location of faces, objects, and landmarks in viewed scenes, whereas in rodents the representations in the hippocampal system are mainly about the place where the individual is located and self-motion between places.

Keywords: hippocampus; memory; spatial scenes; visual cortical streams; “What” and “Where” visual cortical pathways.

Introduction

This research utilizes deterministic dynamical graphs to analyze new effective connectivity measurements between 360 cortical regions in the Human Connectome Project Multimodal Parcellation atlas in 956 HCP participants when viewing spatial scenes, faces, tools, and body parts. Two separate networks are revealed. One is a ventromedial cortical visual “Where” network from V1 to the hippocampus via ventromedial, retrosplenial, and medial parahippocampal scene areas. This network is revealed as separate from the well-known ventrolateral visual cortical “What” network via the fusiform face cortex (FFC) and lateral parahippocampal cortex TF to the hippocampus. These two cortical networks allow separate “Where” and “What” information to be used within the hippocampus for episodic memory and navigation. The specialized cortical ventromedial scene “Where” network for what is encoded about locations “out there” in viewed scenes using spatial view cells is fundamental for understanding primate including human hippocampal function in memory and navigation, for the hippocampal system representations in rodents are primarily about the place where the rodent is located.

The aim of the research described here is to make advances in understanding how whole networks of human visual cortical regions may be linked together and provide inputs to the hippocampal memory system, and how the flow of signal between the visual cortical regions may be different depending on what types of visual stimuli are being viewed. In this research, we start

by measuring effective connectivity with functional magnetic resonance imaging (fMRI) between 180 cortical regions in each hemisphere both during the resting state and when faces, scenes, tools, or body parts are being viewed in 956 Human Connectome Project participants. We then apply graph theory to help define the flow of signal between whole networks of cortical regions. In the deterministic dynamical graph theory approach implemented for this research, the cortical regions are the nodes in the graph, and the effective connectivities are used to define the structure of the directed graph. The graph is directed in that the connectivity in both directions between every pair of nodes defines the edges or connectivity in the directed graph. We show that there is a separate human ventromedial visual cortical network for scenes from the ventrolateral visual cortical network for objects and faces, with both reaching the hippocampal memory system. These “Where” and “What” pathways to the human hippocampus are key to understanding how the human hippocampus operates for episodic memory (Rolls 2023b; Rolls and Treves 2024).

There has been much recent research on the effective connectivity of visual cortical and related regions in humans (Rolls et al. 2023c, 2023e; Rolls 2024b, 2024c) en route to the hippocampal memory system (Rolls 2022, 2023b; Rolls and Treves 2024; Rolls et al. 2025), and on the selective activation of these same regions by different visual stimuli (Rolls et al. 2024e). Effective connectivity measures the effect of each pair of brain regions on each other, using in these investigations the functional connectivity and the lagged functional connectivity measured with fMRI

or magnetoencephalography in humans. The pairwise effective connectivities do not however show how whole networks of cortical regions may be linked together, and how the flow of signal between the cortical regions may be different depending on what types of visual stimuli are being viewed. The research described takes, we believe, a conceptually important step forward by building on the foundation of the pairwise measurement of effective connectivity between each pair of 360 cortical regions in the Human Connectome Project Multimodal Parcellation (HCP-MMP (Glasser 2016a)) that we have analyzed using whole cortex effective connectivity with 360 cortical regions (Rolls et al. 2022a–c; 2023a–g), to the analysis of whole networks of connected cortical regions.

We note that the effective connectivity between the cortical regions does differ depending on what type of visual stimulus is being shown (Rolls et al. 2024e). We make use of this to analyze the flow of signal through the whole networks when different types of visual stimuli are being viewed, including scenes, faces, tools, and body parts.

In the research described here, the cortical regions are defined by the HCP-MMP of the cerebral cortex (Glasser 2016a). The HCP-MMP is a well-founded parcellation of the human cerebral cortex into 360 cortical regions that utilizes evidence from anatomy (cortical thickness and cortical myelin), functional connectivity, and task-related fMRI (Glasser 2016a). This atlas provides a reference system that can be used in many investigations of human cortical function, to provide a reference standard to enable findings from different investigations to be compared. The HCP-MMP (Glasser 2016a) has been extended to include 66 subcortical areas (Huang et al. 2022). The HCP-MMP is the best cortical atlas we know for delineating the smallest functional cortical regions that can be reliably identified with multimodal evidence in humans, which may be building blocks of cortical function and provide a basis for advancing our understanding of cortical function (Rolls 2023a). All the data analyzed were in the surface-based version of the HCP-MMP atlas, as that provides the most accurate identification of each cortical region (Glasser 2016a). It contrasts with many earlier parcellations of the cerebral cortex that are less computationally useful as they are based on gross topology (Rolls et al. 2015, 2020), or on cortical regions categorized primarily by functional connectivity (Power 2011; Schaefer 2018). For example, in contrast to the HCP-MMP, one study (Schaefer 2018) used only functional connectivity to parcellate the human cerebral cortex into 400, 600, 800, or 1,000 cortical regions, each parcel did not have a clear description of its boundaries or label that can be related easily to an anatomically and functionally defined cortical region, and the parcellation is stated to be less good for visual cortical areas (Schaefer 2018) than the HCP-MMP (Glasser 2016a). For these reasons, the surface-based HCP-MMP parcellation (Glasser 2016a) was used here.

The effective connectivity matrices used here were measured between all 360 regions in the HCP-MMP atlas, in either the resting state in 171 HCP participants imaged at 7T as used in previous research (Rolls et al. 2022a, 2023c) (with very similar results in 956 HCP participants imaged at 3T), or when faces, scenes, tools, or body parts were being viewed in 956 HCP participants at 3T (Rolls et al. 2024e). The resting-state effective connectivity matrices were used from this previous research (Rolls et al. 2022a; 2023c) because they use the HCP-MMP parcellation, and because the effective connectivity algorithm used in that research can show the effective connectivities between all 360 cortical regions. The Hopf effective connectivity algorithm used here is described in Sections Methods and Supplementary Material. No other research

we know provides similar analyses of effective connectivity, functional connectivity, and diffusion tractography between these 360 cortical regions, which help to make the present research unique and beyond what has been possible before. For example, another approach to measuring effective connectivity, dynamic causal modeling (Stephan et al. 2007b; Marreiros et al. 2008; Friston 2009; Razi 2017), is typically applied to only a very few, often 3 or 4, brain areas in task-related fMRI (Stephan et al. 2007a; Heim 2009; Schurz 2014).

As an introduction to the cortical systems investigated here, Fig. 1 shows the human brain with the cortical regions defined in the HCP-MMP parcellation atlas (Glasser 2016a), for reference while considering the flows between the visual cortical regions analyzed here. Figure 1 shows a summary of the effective connectivity in the two main visual cortical pathways investigated here, based on previous research which measured effective connectivity and activations in a ventromedial visual cortical pathway for scenes and a ventrolateral cortical visual pathway for objects and faces (Rolls et al. 2022a, 2023c, 2023e, 2024b; Rolls 2024b, 2024c). An aim of the present research is to go beyond what can be demonstrated with effective connectivity by using graph theory to help define separate whole visual cortical networks, and how these whole networks are reshaped depending on the stimuli being shown and therefore the computations being performed (Rolls 2023a). More details of these cortical regions in the HCP-MMP parcellation are provided in Fig. S1 and Table S1.

We note that of course there has been much previous research on human brain activations to faces (Kanwisher et al. 1997; Spiridon et al. 2006; Vul et al. 2012; Weiner and Grill-Spector 2015), scenes (Epstein and Kanwisher 1998; Epstein and Julian 2013; Epstein and Baker 2019; Tsitsiklis 2020), body parts (Pitcher et al. 2011; Vul et al. 2012; Weiner and Grill-Spector 2013; Deen et al. 2015; Orban et al. 2021; Urgen and Orban 2021; Kosakowski 2022; Rolls 2023b, 2024b), and tools (Kastner et al. 2017; Maravita and Romano 2018) etc, but that the aim of the present research here is different, to produce a network graph of the flow of signal between visual cortical regions in the resting state and when different visual stimuli are being shown, and with the HCP-MMP atlas because this atlas provides a well-founded framework for specifying cortical regions and comparing results between investigations. This aim of the present research is important for building a framework for better understanding human cerebral cortex function in health and in disease (Rolls 2023a).

Previous graph-based approaches to understanding cortical connectivity (Fornito et al. 2016; Faskowitz et al. 2022; Betzel et al. 2023; Seguin et al. 2023) have not analyzed bidirectional networks and the flows between their nodes across the whole brain, for directed effective connectivity measures across all 360 cortical regions that can now be identified (Glasser 2016a) have only recently become available (Rolls et al. 2022b, c, 2023a; Rolls 2023a; Rolls et al. 2023b–g; 2024a; Rolls 2024c).

Materials and methods

Measurement of the effective connectivity

Effective connectivity measures the effect of one brain region on another, and utilizes differences detected at different times in the signals in each connected pair of brain regions to infer effects of one brain region on another. One such approach is dynamic causal modeling, but it applies most easily to activation studies, and is typically limited to measuring the effective connectivity between

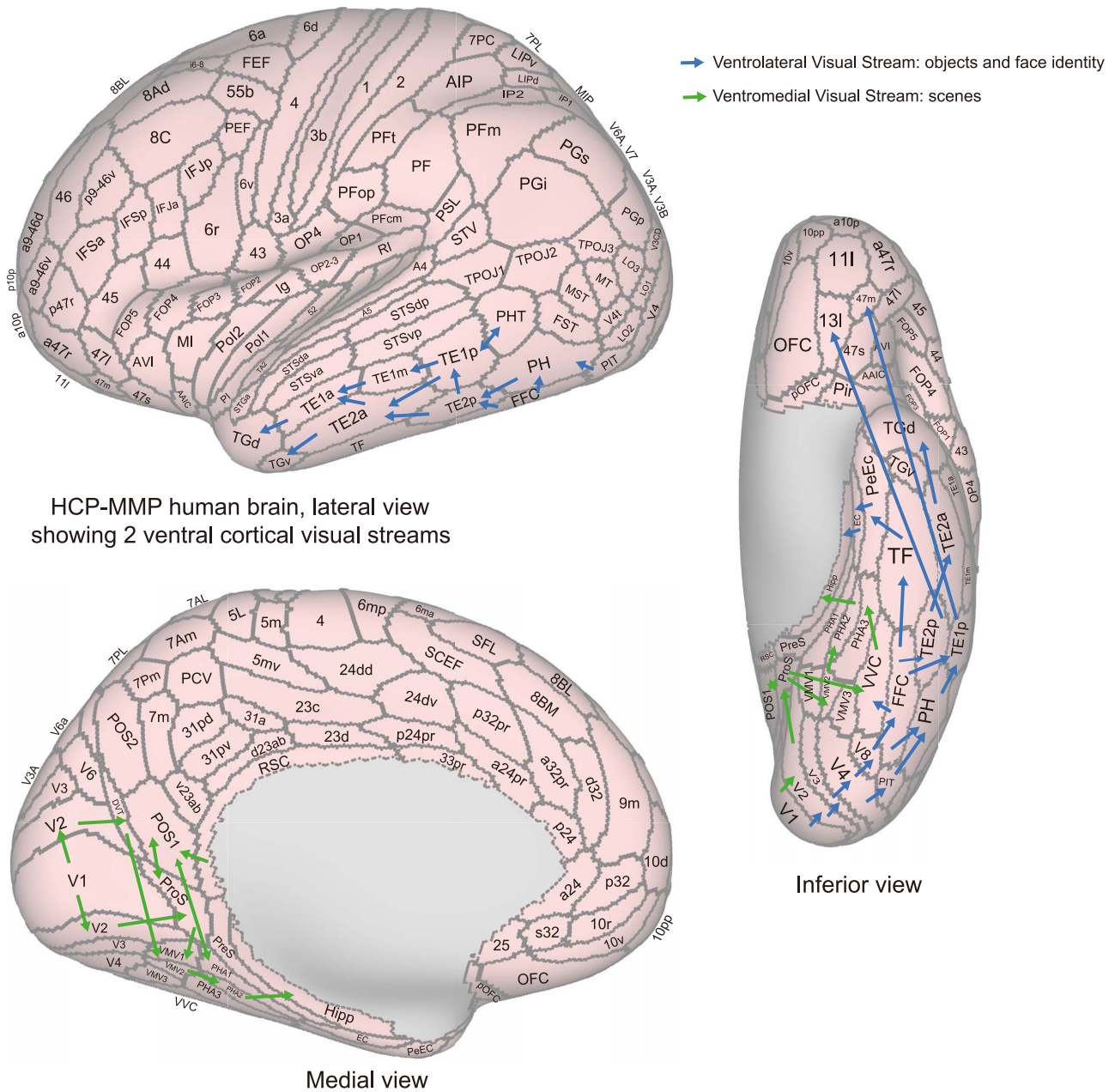


Fig. 1. The 2 visual cortical pathways analyzed here. Effective connectivity has revealed a ventromedial visual cortical pathway for scenes (green arrows), and a ventrolateral visual cortical pathway for objects and faces (blue arrows) (see text and Rolls 2024b). The pathways are shown on the parcellation of the human cortex in the HCP-MMP atlas (Glasser et al. 2016a, 2016b), and in its extended version HCPex (Huang et al. 2022). The regions are shown on images of the human brain in inflated form with the sulci expanded sufficiently to allow the regions within the sulci to be shown. The abbreviations for each cortical region are provided in Table S1, and the cortical regions are illustrated in Fig. S1.

just a few brain areas (Friston 2009; Valdes-Sosa et al. 2011; Bajaj et al. 2016), though there have been moves to extend it to resting state studies and more brain areas (Frassle 2017; Razi 2017). The method used here (Rolls et al. 2022a,c) was developed from a Hopf algorithm to enable measurement of effective connectivity between many brain areas, described by Deco (2019). A principle is that the functional connectivity is measured at time t and time $t+\tau$, where τ was set to 2 s for the relatively slow fMRI BOLD signal. To infer the effective connectivity, we use a whole-brain model that allows us to analyze the fMRI signal across all brain regions and time. We use the so-called Hopf computational model, which integrates the dynamics of Stuart-Landau oscillators, expressing

the activity of each brain region, by the underlying connectivity (Deco et al. 2017b). As mentioned above, we include in the model 360 cortical regions in the HCP-MMP parcellation (Glasser 2016a). The local dynamics of each brain area (node) is given by Stuart-Landau oscillators, which expresses the normal form of a supercritical Hopf bifurcation, describing the transition from noisy to oscillatory dynamics (Kuznetsov 2013). During the last years, numerous studies were able to show how the Hopf whole-brain model successfully simulates empirical electrophysiology (Freyer 2011; Freyer et al. 2012), MEG (Deco 2017a), and fMRI (Kringelbach et al. 2015; Deco et al. 2017b; Kringelbach and Deco 2020; Kringelbach et al. 2023).

The Hopf whole-brain model can be expressed mathematically as follows:

$$(\dot{x}_i)/dt = \overbrace{[a_i - x_i^2 - y_i^2]x_i - \omega_i y_i}_{\text{LocalDynamics}} + \overbrace{G \sum_{j=1}^N C_{ij}(x_j - x_i)}_{\text{Coupling}} + \overbrace{\beta \eta_i(t)}_{\text{GaussianNoise}} \quad (1)$$

$$(\dot{y}_i)/dt = [a_i - x_i^2 - y_i^2]y_i + \omega_i x_i + G \sum_{j=1}^N C_{ij}(y_j - y_i) + \beta \eta_i(t) \quad (2)$$

Equations 1 and 2 describe the coupling of Stuart-Landau oscillators through an effective connectivity matrix C . The $x_i(t)$ term represents the simulated BOLD signal data of brain region i . The values of $y_i(t)$ are relevant to the dynamics of the system but are not part of the information read out from the system. In these equations, $\eta_i(t)$ provides additive Gaussian noise with standard deviation β . The Stuart-Landau oscillators for each brain region i express a Hopf normal form that has a supercritical bifurcation at $a_i = 0$, so that if $a_i > 0$ the system has a stable limit cycle with frequency $f_i = \omega_i/2\pi$ (where ω_i is the angular velocity); and when $a_i < 0$ the system has a stable fixed point representing a low activity noisy state. The intrinsic frequencies are fitted from the data, as given by the averaged peak frequency of the narrowband BOLD signals of each brain region. The intrinsic frequency f_i of each Stuart-Landau oscillator corresponding to a brain region i was in the 0.008–0.08 Hz band ($i = 1, \dots, 360$) for the HCP fMRI data used here, which was sampled at $TR = 0.72$ s. The coupling term representing the input received in node i from every other node j , is weighted by the corresponding effective connectivity C_{ij} . The coupling is the canonical diffusive coupling, which approximates the simplest (linear) part of a general coupling function. G denotes the global coupling weight, scaling equally the total input received in each brain region. While the oscillators are weakly coupled, the periodic orbit of the uncoupled oscillators is preserved.

The effective connectivity (C) matrix is derived by optimizing the conductivity of each connection in the matrix in order to fit the empirical functional connectivity ($\mathbf{FC}^{\text{empirical}}$) pairs and the lagged normalized covariance, the $\mathbf{FS}^{\text{empirical}}$ pairs. By this, we are able to infer a nonsymmetric effective connectivity matrix (see Gilson et al. (2016)). We refer to this as a generative effective connectivity model approach because the C matrix is used to generate the functional connectivity and lagged normalized covariance matrices, and the C matrix is optimized so that the simulated matrices match the empirically measured matrices. Note that $\mathbf{FS}^{\text{empirical}}$, ie the normalized lagged covariance of the functional connectivity between pairs, lagged at τ , breaks the symmetry and thus is fundamental for our purpose. Specifically, we compute the distance between the model functional connectivity $\mathbf{FC}^{\text{model}}$ calculated analytically from the current estimate of the effective connectivity and the empirical data $\mathbf{FC}^{\text{empirical}}$, as well as the calculated model $\mathbf{FS}^{\text{model}}$ and empirical data $\mathbf{FS}^{\text{empirical}}$ and adjust each effective connection (entry in the effective connectivity matrix) separately with a gradient-descent approach. The model is run repeatedly with the updated effective connectivity until the fit converges towards a stable value.

The effective connectivity matrix C_{ij} can be initialized with the anatomical connectivity obtained with probabilistic tractography from diffusion MRI, or the matrix can be initialized to zero. For all the research described by the senior author, the effective connectivity matrices shown were initialized to 0, because use of the structural connectivity matrix could limit the connectivity to

fewer links than are otherwise found with these fMRI data, probably because the tractography analysis missed some connections; and the algorithm converges well when the effective connectivity matrix C_{ij} is initialized to 0. However, the correlation between the matrices produced with these different methods was reasonable (0.80). In addition, the directions of all the effective connectivities in all of this fMRI research were reversed, because this aligns the results with what is found with the much faster neuroimaging method magnetoencephalography (Rolls et al. 2023e; Rolls 2024c). The necessity for this reversal of direction with slow fMRI data is that for most of the $\tau = 2$ s period used with fMRI, the input has progressed from early cortical regions within 200–300 ms, and so for most of the 2 s period the signal is backprojecting top-down from higher cortical regions where short-term memory may be implemented to early cortical regions (Rolls et al. 2023e; Rolls 2024c). Another point is that the effective connectivity can alternatively be calculated analytically, with the analytic method described in Supplementary material and elsewhere (Rolls 2024c).

This effective connectivity approach has been used extensively, and indeed the resting-state effective connectivity matrix utilized here was from 171 HCP participants at 7T (Smith 2013; Van Essen 2013) and was the same as that utilized in the analysis of the effective connectivity of most cortical systems in humans (Rolls et al. 2022a–c; 2023a–d, 2023f, 2023g; 2024a). For the task-related effective connectivity matrices utilized here for the analysis of connectivities associated with viewing faces, scenes, tools, and body parts, the data used to compute the new effective connectivities utilized here were from 956 HCP participants imaged at 3T in the 0-back memory task (Barch 2013) that were extracted and utilized in the analysis of activations and functional connectivities in these participants that are described in detail elsewhere (Rolls et al. 2024b). In more detail, the data with visual stimuli are from 956 participants in the Human Connectome Project Working Memory Task (Barch 2013), in which runs consisted of 10 presentations of scenes or faces or body parts or tools presented for 2 s each and separated by a 0.5 s gap (Rolls et al. 2024b). The preparation of the data has been described elsewhere (Rolls et al. 2024b). As shown in Fig. 1 of Rolls et al. (2024b), each run for 10 presentations of 1 type of stimulus (eg scenes) lasted for 25 s, and that provided the data for each run. Data only for the 0-back memory condition were used, to minimize the memory load but to ensure that the participants were viewing and processing the visual stimuli. The effective connectivity was measured from the 3 runs available from each participant for each of the 4 types of visual stimuli, using the same Hopf algorithm as used previously (Rolls et al. 2022a, 2023e; Rolls 2024c) and that is also described for the analytic version in Supplementary material. An example of an effective connectivity matrix is shown for completeness in Fig. S2.

Overview of the dynamical graph approach

The effective connectivity provides bidirectional asymmetric connectivity between every pair of the 180 nodes in each hemisphere. Taking the effective connectivity matrices for all 360 cortical regions in the HCP-MMP atlas referred to above, the approach taken here was to measure the flow of signal in a graph of the visual cortical regions, which are the nodes in the network. To measure the flow of signal, we first define a propagation matrix P using the effective connectivity matrix. The propagation matrix measures the proportion of signal from any one node in the system that can flow to all other nodes in the system, and provides that for all nodes in the system. In the formulation described here for the brain, the signal that reaches a node does not diminish

with time. An input of value 1 is then applied at every timestep to 1 (or more) nodes in the network (in this case the primary visual cortex, which therefore becomes the source for the network), and at subsequent timesteps the activation (or signal S below) that is produced in each node is calculated by the activation in the previous timestep of the nodes *from which* it receives multiplied by the propagation matrix. The flow of signal *out of the nodes* in the network at each timestep can then be calculated by multiplying the activations in the nodes at each timestep by the propagation matrix.

We note that there has been much previous research on the application of graph theory to understanding brain networks (Sporns et al. 2005; Fornito et al. 2016; Seguin et al. 2023), but that much has focussed on the properties of the adjacency matrix which defines whether nodes are connected, such as in-degree, out-degree of nodes, centrality, hub nodes, etc., reflecting mostly the static characteristics of these networks (Fornito et al. 2016), though diffusion processes are considered in Chapter 7 of Fornito et al. (2016). In contrast, here we focus on a measure of flow that is deterministic and in a system where once a node is activated, its activation continues and reflects the activations at the previous timestep in the nodes from which it receives input weighted by the propagation matrix. Further, we go beyond these properties of adjacency matrices to investigate how particular nodes are related to each other, in order in particular to study the flow of signal from node to node through a whole network of brain nodes. We also emphasize that the approach here is deterministic in how the signal propagates through the graph over time, and that is different from random walk approaches that model diffusion processes (Doyle and Snell 1984; Fornito et al. 2016).

In the research described here, the main interest was in the flow of signal after sufficient time for the signal to reach and equilibrate in the last node defined in the network, the hippocampus. This was typically 40 timesteps for the task-related flows, and up to 100 timesteps for the resting state flows. The cortical regions included in the graph from the HCP-MMP atlas were chosen based on known cortical visual regions and their activations found to visual stimuli (Rolls et al. 2024e) and on previously measured effective connectivities from V1 onwards towards the hippocampus (Rolls et al. 2022a; 2023c, 2023e; Rolls 2024b). The cortical regions en route to the hippocampus chosen for this investigation were V1, early cortical visual regions V2, V3, V4; ventrolateral visual cortical stream regions V8, PIT, and FFC, and the lateral parahippocampal gyrus TF; ventromedial visual cortical stream regions ProStriate cortex ProS, VMV1, VMV2, VMV3, VVC, and the medial hippocampal gyrus PHA1, PHA2, and PHA3; and the perirhinal cortex, entorhinal cortex, and hippocampus (see Fig. 1). However, it should be noted that when calculating these graphs, all 180 regions in the left hemisphere were included in the calculations, so the flow between some of the nodes in the graphs shown here could reflect signals in other connected nodes.

In the following, we provide the details of how the signal flow graphs between nodes were calculated and how the whole network was thereby revealed.

The main focus of our study is a description of the pathways of signal through a network of N nodes with a given strength of the directed connections, measured by the effective connectivity (EC) between every pair of nodes. As the size N of the network is rather large (it is 90–180), a list of all the pathways becomes too vast to be tractable. We suggest a straightforward simple procedure (based on the linear dynamics in \mathbf{R}_+^N) to get the major effective pathways. We apply this method to describe the graphs of the flow of signals in the visual cortical regions defined above.

It can be noted that although 180 nodes is too high a number to draw and to visualize all the paths in a network, it is still too small to apply (indeed, commonly used but without estimating an actual error) results of random graph theory. Furthermore, given that each connection in the matrix that we treat here has a particular meaning, a randomization would be inappropriate in this setting. Instead we suggest a simple method of considering networks with graded connections for increasing complexity and precision of the underlying graphs. When we calculate the flow between the nodes shown in the figures, the algorithm calculates the flows based on all 180 nodes in the network.

Model of propagation of signals in a network.

The network is composed of N brain regions. Each node $1 \leq i \leq N$ of a network represents a brain region i .

The connections between all nodes are given by the EC matrix, introduced above and described in [Supplementary material](#). We denote this matrix

$$\mathbf{E} = (E_{ij})_{1 \leq i, j \leq N}.$$

Note that the elements E_{ij} of this matrix are non-negative numbers, and each E_{ij} represents a strength of a connection *from node j to node i* , which is consistent with what we use for effective connectivity (Rolls et al. 2022b, 2022c; 2023a–g; 2024a; Rolls 2024c).

Given matrix \mathbf{E} let us introduce the flow of an external signal through a network from the input. We consider a discrete time dynamics, $t = 1, 2, \dots$. The strength of signal at node i at time t is denoted by $S_i(t)$, which takes non-negative values. The dynamics of the state of network $S(t) = (S_i(t), i = 1, \dots, N)$ is defined as follows. Let matrix \mathbf{C} denote \mathbf{E} transposed, that is $C_{ij} = E_{ji}$.

At time $t = 1$ a subset $I \subset \{1, \dots, N\}$ of nodes receives an external input $X > 0$, which means that

$$\begin{aligned} S_i(1) &= X & i \in I, \\ S_i(1) &= 0 & \text{otherwise.} \end{aligned} \quad (3)$$

Then the dynamics of $S(t)$ describes the flow of a signal from the initial input set I . If $S_i(t) > 0$ then the signal from node i to node j propagates through the out-coming edge ij (if $C_{ij} > 0$) increasing the value of $S_j(t + 1)$. The direction and the strength of this flow through the edges of matrix \mathbf{C} are determined by a propagation matrix \mathbf{P} defined as follows:

$$P_{ij} = \frac{C_{ij}}{\sum_j C_{ij}}. \quad (4)$$

This is a natural definition for a propagation matrix used to set up the dynamics that specifies the proportion of the output of a signal from a node that propagates to each output edge or link from that node, which preserves the amount of signal in the system. As a transposed of \mathbf{P} has properties of a stochastic matrix (in terms of definition in algebra), that is $\sum_j P_{ij} = 1$ vector $(1, \dots, 1)$ is invariant for our system, the system converges to an equilibrium of $(1, \dots, 1)$ as is seen in Fig. 9.

The external signal $I(t)$, $t \geq 1$, into a network comes through nodes in I . Typically $I(t)$ is given by a step function

$$I(t) = \begin{cases} X, & t \leq T, \\ 0, & t > T, \end{cases} \quad (5)$$

where T is a duration of a constant input X .

In the analyses described here, X was typically set to 1 in node 1 the primary visual cortex V1 (ie $I = \{1\}$) for the whole duration of each run. Further, the value of signal $S_1(t)$ for node V1 was clamped to 1, to reflect strong visual input to it and to prevent its activation being built up by flows back to it which would lead to increasing flows throughout the system as a function of the number of timesteps. Because there is some flow in the backprojection direction to V1, the activation of V1 might over time build up, so clamping this at 1 prevents any positive feedback runaway effects of this type. In the cortex, it is proposed that this function is implemented by strong feedback inhibition by inhibitory neurons, and also by processes such as neuronal and synaptic adaptation (Rolls et al. 2024d).

Given the state $S(t) = (S_i(t), i = 1, \dots, N)$, ie, the vector of amount of signal in each node for $t \geq 1$, the state of the network in the next moment of time is defined by the following linear system

$$\begin{cases} S_1(t+1) = 1, \\ S_j(t+1) = \sum_i S_i(t)P_{ij}, \quad \text{if } j \neq 1. \end{cases} \quad (6)$$

Typically in the analyses described D is set to be the node for the hippocampus, and it is treated as any other node, allowing activation to build up in node D , and to potentially be reflected backwards through the network (depending on the propagation matrix derived from the effective connectivity matrix).

The focus of our study is the flow of signal in the network. The amount of signal passing from node i to node j at time t in system (6) is defined by

$$F_{i,j}(t) = S_i(t)P_{ij}. \quad (7)$$

Correspondingly, we can visualize the matrix of flow $F(t) = (F_{ij}(t))_{1 \leq i,j \leq N}$ as a graph with edges with a width that reflects the flow, ie where the width of edge (ij) is related to the value $F_{ij}(t)$. Observe that although $F(t)$ is derived from the connectivity matrix, analysis of its dynamics in time as a function of the input enhances the information derived solely from the connectivity matrix. It is emphasized that $F_{ij}(t)$ depends polynomially on the effective connectivity matrix \mathbf{E} .

Selection of nodes for the flow graph

In the analyses described here, we are especially interested in analyzing the subgraphs (pathways, or separate cortical streams) from the primary visual cortex V1 via, which signal can reach the hippocampal memory system. We therefore chose the key nodes in the ventrolateral visual cortical pathways and the ventromedial visual cortical path for the analyses (Rolls 2024b). These nodes as set out above were V1, early cortical visual regions V2, V3, V4; ventrolateral visual cortical stream regions V8, PIT, and FFC, and the lateral parahippocampal gyrus TF; ventromedial visual cortical stream regions ProStriate cortex ProS, VMV1, VMV2, VMV3, VVC, and the medial hippocampal gyrus PHA1, PHA2, and PHA3; and the perirhinal cortex, entorhinal cortex, and hippocampus (see Fig. 1). We are also interested in analyzing how the signal flows develop over time in the network, and accordingly we also investigate the flows after different numbers of timesteps t . The flow graphs were visualized with the Matlab function `plot()`. In the flow graphs in the figures, small flows are not shown, in order to keep clear the structure of the flow graph. The threshold for this display simplification is shown in the figure legends.

Assessment of the differences of the flows for different visual stimuli

To provide a guide to the flows that were different when different visual stimuli were being performed, a 4-way data split was performed across the 956 participants, to produce four randomly selected groups each with 239 different participants. The effective connectivities were calculated for each of these data splits, and for each split the flows for each stimulus type (faces, places, tools, body parts) were then calculated. Then t-tests were performed to test for which pairs of brain regions had different flows between them when for example faces were compared with scenes. The means across the right and left hemispheres are reported. The results are presented after FDR correction for multiple comparisons, using $P \leq 0.01$ after the FDR correction has been applied. Six preplanned statistical comparisons were performed for the flows in the ventromedial cortical “Where” stream VMV1-3 and VVC, and in the ventrolateral “Where” stream FFC. To limit the number of regions listed in the reports, differences of flow are only reported where the difference was ≤ 0.01 (with the maximum flow ~ 0.1).

Results

First the flow is shown in both directions between all the selected nodes from V1 to the hippocampus based on the effective connectivity measured in the resting state. Then the flow is analyzed when the effective connectivity was measured while participants were performing a visual 0-back memory task for scenes, faces, tools, or body parts, to show how the flow in the network was different when different types of visual stimuli are being processed.

The visual cortical network in the resting state

Figure 2 shows the flow between V1 and the hippocampus based on the resting state connectivity, which was measured with fMRI in 171 participants at 7T as previously described (Rolls et al. 2022a; 2023c) with HCP data (Smith 2013; Glasser 2016b). The resting-state effective connectivity is sometimes thought to reveal the basic connectivity of the cerebral cortex when it is not having to respond to external stimuli. The effective connectivity matrix obtained was reliable in that it was correlated 0.935 with the effective connectivity matrix that we calculated from 956 HCP participants at 3T. The time delay used in the calculation of effective connectivity was $\tau = 2$ s, so there was plenty of time for the signal to have freely circulated between all the nodes analyzed, given the speed of processing of ~ 15 ms from region to region based on research in macaques (Rolls 2023a), and on imaging with the much faster method of magnetoencephalography (Rolls et al. 2023e). As described in Section Methods, the graph of flow was constructed using the 7T effective connectivity matrix, and a signal of 1 was applied to V1 at every timestep of the flow algorithm described in Section Methods and the activation of V1 was clamped at 1. The flows shown in Fig. 2 were calculated after 100 timesteps, which allowed ample time with this resting state data for the signal to reach the hippocampus. The activations S in each of the nodes are indicated by color as described in the figure legend.

Figure 2 shows the flow as stronger r from V1 to its closely connected regions than vice versa, including V2 (forward flow = 149, reverse flow = 23), V3 (forward flow = 117, reverse flow = 12), V4 (forward flow = 60, reverse flow = 4), and V8. Similarly, the flow is stronger from V2 to V3 and V4, etc. than vice versa. Similarly, the flow is in general stronger from these cortical visual

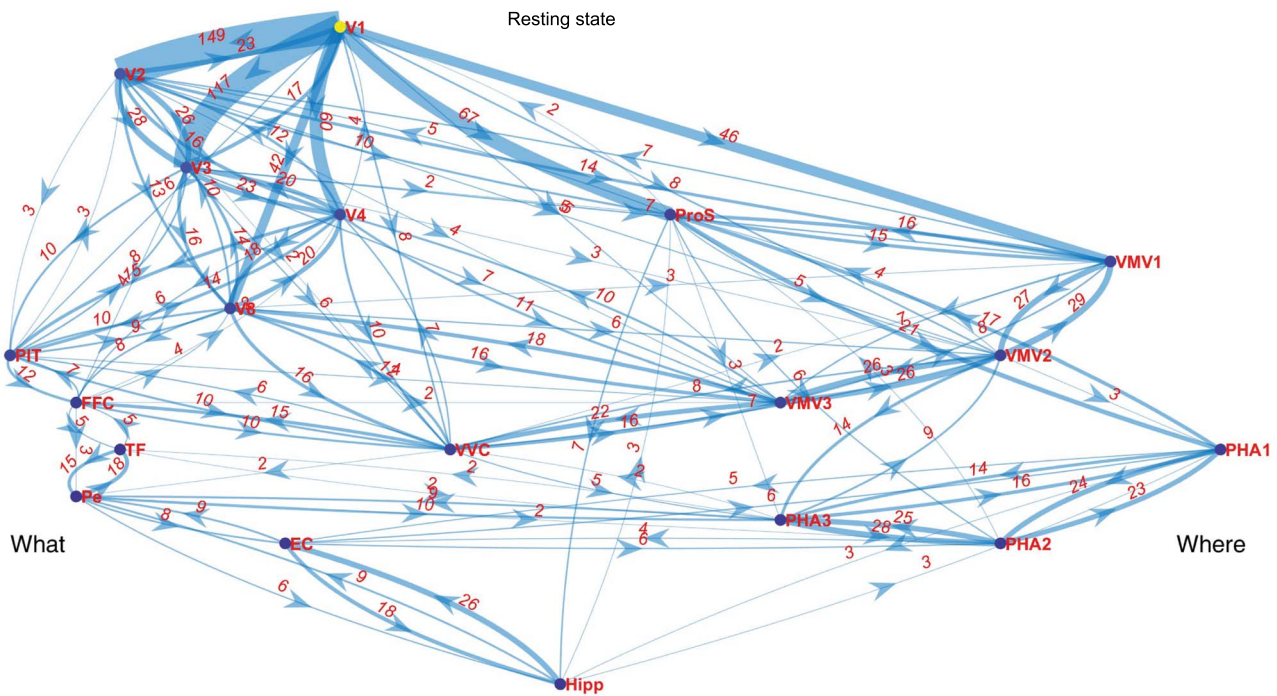


Fig. 2. Visual cortical networks in the resting state with 171 HCP participants at 7T. The flows F measured at time = 100 are indicated by arrows with numbers close to the arrows, and the width of the arrows represents the strength of the flow. Because the flows are lower for these visual cortical regions in the resting state than when visual stimuli are being shown, for this figure only, the Flows F were measured at time = 100, and the flows were thresholded at 2 to clarify the figure by not showing small flows. The flows in each direction are indicated by the numbers close to the curved edges, and if one of the flows is <2 , a single straight arrow is shown between a pair of nodes. The activations S in each of the nodes are indicated by color from yellow as the highest to dark blue as the lowest. The ventrolateral cortical visual “What” stream is on the left, and the ventromedial cortical visual “Where” stream is on the right.

regions to V8, PIT (posterior inferior temporal cortex), and FFC. (To help appreciate these flows, the visual cortical regions in Fig. 2 are set out in an order that may correspond to the order of regions in the hierarchy based on their location in the human brain, their pairwise effective connectivity, and neuroanatomical evidence from macaques (Felleman and Van Essen 1991; Markov 2014; Van Essen and Glasser 2018), with V1 at the top, V2 at a step down on the vertical axis, V3 at the next step, followed by V4, V8, PIT, FFC, TF, Pe [perirhinal cortex], EC [entorhinal cortex], and then the hippocampus [Hipp].) From FFC to the hippocampus, the flows are more equal in both directions or indeed reversed from the hippocampus backwards, which may be consistent with the backprojections from the hippocampus being important in memory retrieval (Treves and Rolls 1994; Rolls and Treves 2024). This corresponds to a ventrolateral visual cortical “What” stream to the hippocampus (Rolls 2023b; 2024b).

There is also stronger flow from V1 to the ProStriate cortex (ProS) than vice versa (forward flow = 67, reverse flow = 2), and to ventromedial cortical visual region VMV1 (forward flow = 46, reverse flow = 0), which it is proposed are the start of the ventromedial cortical visual “Where” stream for visual scene information to reach the hippocampus (Rolls 2023b; 2024b).

An important point from Fig. 2 is that the flows in the stream or network just described on the left in Fig. 2 (sometimes termed a “What” network (Mishkin et al. 1983; Rolls and Treves 2024; Rolls 2024b)), are generally separate from those in what is to some extent the separate network on the right of Fig. 2, the “Where” network. More evidence that these streams are somewhat separate is provided in Figs. 3–6 when different flows are found in these streams when faces, scenes, tools or body parts are being viewed.

The network on the right of Fig. 2 shows what has been described as a ventromedial visual cortical stream for information about visual scenes represented by spatial view cells in the medial parahippocampal gyrus PHA1–PHA3 and hippocampus in primates including humans, and has accordingly been termed a “Where” pathway (Rolls 2023b; Rolls and Treves 2024). In this pathway there is strong flow directed to the ProStriate cortex ProS, a region just anterior to V1, and a region that is activated by viewing scenes and is approximately where the retrosplenial place area PPA is found (or better retrosplenial scene area, for it represents the location being looked at in a scene in primates including humans, not the place where the individual is located (Sulpizio et al. 2020; Rolls 2023b; Rolls et al. 2024b; Rolls 2024b)). There is also moderate flow from V2 to ProS (forward flow = 10, reverse flow = 0). ProS in turn has moderate flow with the most medial regions, ventromedial VMV1 and medial parahippocampal PHA1 (see Figs. 1 and 2). VMV1–VMV3 have strong flow with each other, essentially providing for flow from medial to lateral (VMV1, then VMV2, then VMV3), with then moderate flow to the more lateral VVC (Fig. 2) which is adjacent to FFC and a somewhat intermediate region between the ventrolateral “What” and Ventromedial “Where” streams (see Fig. 1).

The visual cortical network when viewing scenes

Figure 3 shows the flow from V1 measured from the effective connectivity matrix when scenes are being viewed, and should be compared with the flow matrix for faces in Fig. 4, for tools in Fig. 5, and for body parts in Fig. 6. The flows in these figures can be directly compared with each other as they were computed from HCP data obtained in the same set of 956 participants at the same time, and were calculated with the same flow algorithm and the

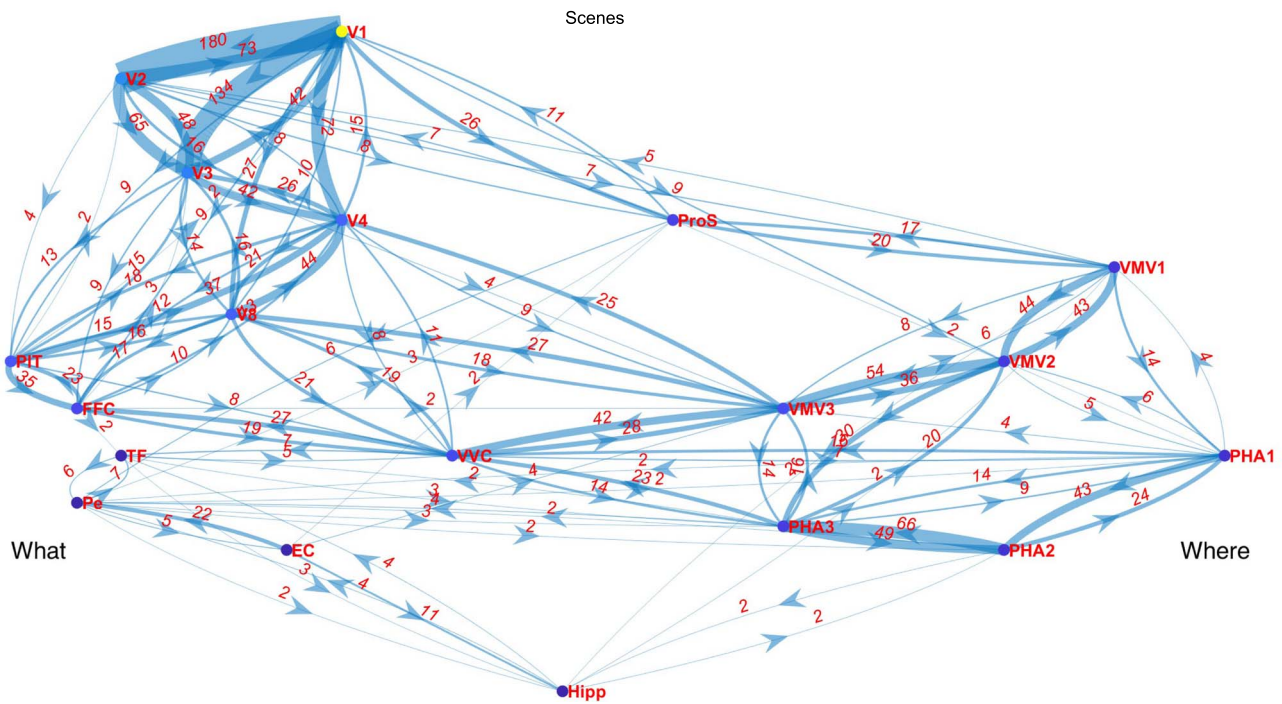


Fig. 3. Visual cortical networks for spatial scenes with 956 HCP participants. The conventions are as in Fig. 2, except that the flows were measured at time = 40. The activations S in each of the nodes are indicated by color from yellow as the highest to dark blue as the lowest. The ventrolateral cortical visual “What” stream is on the left, and the ventromedial cortical visual “Where” stream is on the right.

same number of timesteps, which were sufficient for the flows to be evident in the hippocampal system.

The flows for scenes in Fig. 3 show a ventromedial visual cortical network that is activated, with flows evident in a network from V1 and V2 to the ProStriate cortex (ProS), then to ventromedial cortical region 1 (VMV1) (which also receives flow from V2). VMV1 then has flows to medial parahippocampal PHA1, and VMV2 that has flows with PHA3. VMV2 also has flows with VMV3 that also has flow with PHA3, and with VVC which is strongly coupled to this ventromedial stream when viewing scenes. The ventromedial cortical visual stream then has flow to the hippocampal system in part directly from VMV1 and PHA2 to the hippocampus; and also via entorhinal cortex (EC) from VVC; and also via perirhinal cortex (then entorhinal cortex) from PHA1, PHA2, and PHA3 (Fig. 3).

It is very noticeable that when viewing scenes (Fig. 3) there is much less flow than when viewing faces (Fig. 4) in the “What” ventrolateral visual cortical stream to the hippocampus in key nodes such as V8, PIT, FFC, TF, Pe, and EC to the hippocampus. Moreover, when viewing faces (Fig. 4), VVC has stronger flows with the “What” stream, whereas when viewing scenes VVC has stronger flows with the ventromedial “Where” stream (Fig. 3). This is consistent with the intermediate topological location of VVC between the “What” stream laterally and the “Where” stream medially (Fig. 1).

For comparison, the flows between the corresponding cortical regions in the right hemisphere are shown in Fig. S3. In the right hemisphere, there is for example more flow in parts of the “Where” ventromedial cortical visual network in the right hemisphere, for example in the flow from medial parahippocampal region PHA2 to the hippocampus (Fig. S3). The left–right hemisphere differences in effective connectivity for scenes, faces, tools, and body parts are of considerable interest, and will be considered in detail in future.

The visual cortical network when viewing faces

Figure 4 shows the flows from V1 towards the hippocampus using the effective connectivity matrix when faces are being viewed. The flows are substantial in the ventrolateral “What” cortical stream from V4 in part via V8 and PIT to the FFC; then from FFC via TF (lateral parahippocampal gyrus) to perirhinal (Pe) to entorhinal cortex and thereby to the hippocampus.

Very interestingly, when viewing faces compared to viewing scenes, V4 now has flow almost exclusively with the ventrolateral “What” system with little flow to the ventromedial “Where” system, helping to reveal that the “What” and “Where” systems can operate considerably independently. Also interestingly, VVC now has more flow associated with the ventrolateral “What” network than the ventromedial “Where” network, and indeed for faces provides a route to FFC and TF and even to perirhinal cortex that is additional to the route from V4 via V8 and FFC to TF. Thus, VVC is an interesting region, that can take part in the ventrolateral “What” system or the ventromedial “Where” system depending on the stimuli being viewed, faces in Fig. 4 or scenes in Fig. 3. This fits with the intermediate topological location of VVC in the cortical hierarchies, for VVC is between the ventromedial visual cortical regions VMV1–3 plus PHA1–3, and the ventrolateral cortical stream region FFC (see Fig. 1). These flows also relate interestingly to the activations of VVC, which can be activated by either faces or scenes depending on whether faces or scenes are being viewed (see Fig. 3 of Rolls et al. (2024b)).

Thus a key difference when comparing flows for faces (Fig. 4) compared to scenes (Fig. 3), is that for faces the “What” network is relatively disconnected from the “Where” visual cortical stream, especially by weaker flows from V4 and VVC to the ventromedial “Where” network. Another key difference is that the flows are stronger for faces than for scenes in key nodes in the ventrolateral visual cortical stream such as V8, PIT, FFC, TF, Pe, and EC to the hippocampus.

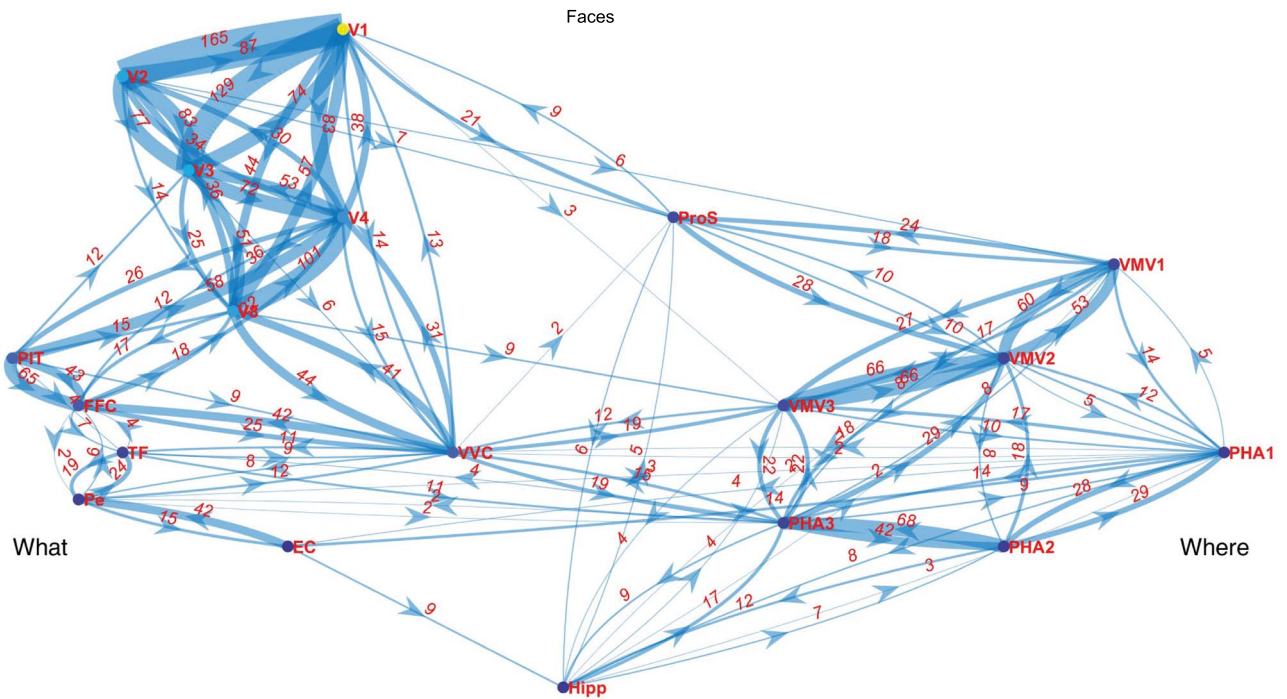


Fig. 4. Visual cortical networks for faces with 956 HCP participants. The conventions are as in Fig. 3.

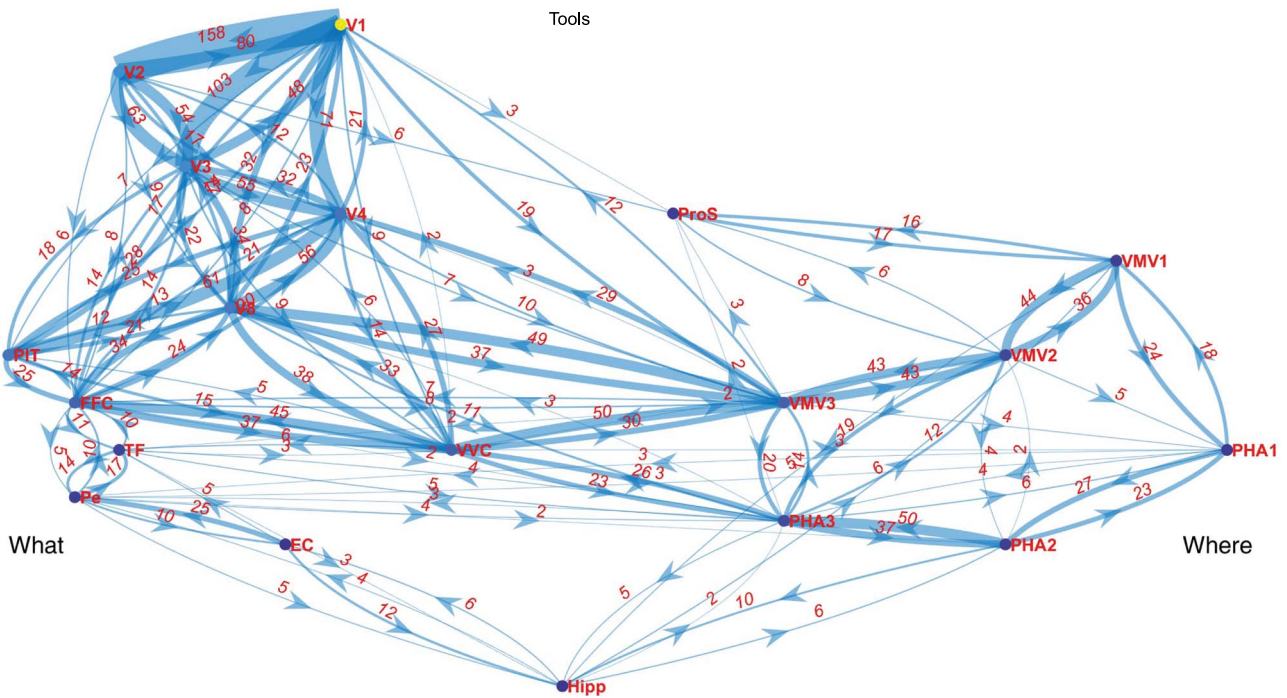


Fig. 5. Visual cortical networks for tools with 956 HCP participants. The conventions are as in Fig. 3.

The visual cortical network when viewing tools

Figure 5 shows the flow from V1 towards the hippocampus using the effective connectivity matrix when tools are being viewed. For tools (compared to scenes in Fig. 3) there is relatively little flow from V1 and V2 to the the ProStriate Cortex (ProS), the start of the ventromedial cortical “Where” stream. Instead, the flows for tools are more via V3, V4 > V8 > PIT and VVC > FFC and VVC and then > perirhinal cortex > entorhinal cortex > hippocampus. VVC for tools provides flows between the ventrolateral “What” and

ventromedial “Where” cortical visual streams to the hippocampus; and another route to the lateral parts of the ventromedial stream is V1 > VMV3 > PHA3. (Here “>” signifies a flow from one brain region to another, though this is not necessarily a unique route.)

When viewing tools, the flows are thus primarily in the ventrolateral “What” network. This relates well to the activations found when tools are being viewed (Rolls et al. 2024b), which are high in VVC, then in VMV3 and PHA3 (which are relatively lateral for

the VMV and PHA regions, see Fig. 1), and then in FFC and TE2p, which is part of the ventrolateral “What” cortical visual stream.

The visual cortical network when viewing body parts

Figure 6 shows the flow from V1 towards the hippocampus using the effective connectivity matrix when body parts are being viewed. The ventrolateral “What” network has strong flows when viewing body parts, with pathways involving V2, V3, V4, V8, PIT, and FFC having high flows, and thereby flows to the hippocampus via TF, perirhinal cortex, and entorhinal cortex (Fig. 6). This is consistent with the activations to body parts, which are high for FFC, TF, and TE2p in the ventrolateral cortical visual “What” stream (Rolls et al. 2024b).

It is also interesting that associated with these strong flows towards the hippocampus from the ventrolateral “What” regions there is some flow back from the hippocampus to regions in the ventromedial “Where” stream such as medial parahippocampal PHA3, then PHA2 then PHA1; and via these regions to ventromedial visual cortical regions VMV1–3 and VVC. Further, there is flow back to ProS, which in turn has flow back to V1. However, these flows in the ventromedial visual cortical stream are not sufficient for this “Where” stream to be activated by body parts (Rolls et al. 2024b).

The flows when there is a short-term memory near the top of the hierarchy

When measuring effective connectivity with fMRI, the connectivities may be in the reverse direction to those measured with magnetoencephalography (Rolls et al. 2023e; Rolls 2024c), and to those expected given that the main input to the primate visual cortical visual system is received in V1. A possible reason for this is the low temporal resolution used with fMRI which is in the order of 2 s to measure a difference in the BOLD signal (Rolls et al. 2023e; Rolls 2024c). It is likely that the signal reaches higher cortical visual areas and the hippocampal system from V1 in less than 200 ms in humans (Rolls et al. 2023e). If after the signal has reached higher cortical visual regions the signal tends to remain high for further processing (using local recurrent collateral attractor networks (Rolls 2023a) and partly perhaps through connectivity with prefrontal short-term memory regions (Rolls et al. 2023d)), then high signal at the top of the hierarchy may tend to have top-down backprojection effects for the rest of the 2 s period (Rolls 2023a) while the effective connectivity is being measured with fMRI. This could result in the effective connectivity being measured by slow fMRI being in the reverse direction (Rolls et al. 2023e; Rolls 2024c).

To investigate how this might affect the flow of signals in the networks described here, a signal of 1 was added to the hippocampus node for every timestep of the simulation for the scene illustrated in Fig. 3. Adding 1 to the hippocampal node simulates a memory recall condition, with activity being recalled in the hippocampal memory system when an incomplete recall cue is completed to a whole memory, and recall of the memory back to the neocortex then occurs (Rolls and Treves 2024; Rolls et al. 2024d). The result is shown in Fig. 7. It can be seen that many of the flows are now in the reverse direction, including PHA3 to VMV3, VMV3 to V4, VMV1 to ProS, and ProS to V1.

This finding is consistent with the hypothesis set out above that a short-term memory high in the hierarchy produces effective connectivities in the reverse direction with fMRI, in the context

of the effective connectivities that were actually measured. It should be noted that in all of our papers with fMRI and the Hopf effective connectivity algorithm, this necessary correction to the effective connectivities was made (Rolls et al. 2022b, 2022c; 2023a–d, 2023f, 2023g; 2024a), and that this was of course not required when the effective connectivities were measured with magnetoencephalography and a τ of 20 ms (Rolls et al. 2023e; Rolls 2024c).

The development of the flows over time

At each timestep of the graph flow algorithm, the flow moves from node to node, as shown in Section Methods. Given that the source node is V1, after a few timesteps, and depending on which nodes have effective connectivity with each other and its strength, the flow should have reached part of the way through the graph of connectivity away from V1. This is investigated by showing in Fig. 8 the flows after 5 timesteps when scenes are being viewed. It is evident that the flows have reached only as far as FFC in the ventrolateral “What” stream, and PHA1–3 in the ventromedial “Where” stream, that all of the flows are stronger away from V1, and that the flow has not reached the entorhinal cortex and the hippocampus. This helps to make it clear how the graph-based approach can be useful in understanding networks in the brain, for the order in which the nodes are activated, and the strength of their activation, is governed by the empirically measured effective connectivities. This can be used to help define which is the “forward” direction of flow, away from V1, by analyzing the graph after different numbers of timesteps.

If the graph is investigated after a large number of timesteps, the flow will have reached the end of the graph (the destination node, in this case the hippocampus), and at each stage of the connectivity, after a node has become active, it can by the empirically measured backward effective connectivity, produce some flows backwards through the network, back towards the source node, V1. This is investigated by showing in Fig. 9 the flows after 1,000 timesteps when scenes are being viewed. The activations and flows are now much higher, as expected, but the direction of the mean flow between some nodes has changed. For example, for spatial scenes, at timestep 40 the forward flow from V1 to ProStriate Cortex is 26, and in the backward direction is 11 (Fig. 3). However, after 1,000 timesteps the forward flow from V1 to ProStriate cortex is 26, and in the backward direction is 57 (Fig. 9). In another example, at timestep 40 the forward flow from V1 to V2 is 180, and in the backward direction is 73 (Fig. 3). However, after 1,000 timesteps the forward flow from V1 to V2 is 180, and in the backward direction is 185 (Fig. 9). This graph approach thus shows how because some of the edges in the graph have effective connectivity in both directions, then after the activations have built up in nodes further from V1, the net flow will start to flow backwards. The exact effects will of course depend on the connectivities throughout the whole 180 nodes in the graph in the left hemisphere that are used to calculate the flows. This is a very useful feature of this graph-based approach to the flow between brain regions, and helps to elucidate the points made above about the reverse effective connectivities that appear to be measured with fMRI with its relatively large τ of 2 s (Rolls et al. 2023e; Rolls 2024c).

It is evident from Fig. 8 that the flows are mainly in the forward direction, away from V1, during the first 5 timesteps, and that some of the flows such as those between V1 and the ProStriate cortex are in the backward direction towards V1 after 1,000 timesteps (Fig. 9). To investigate when and how the flow can

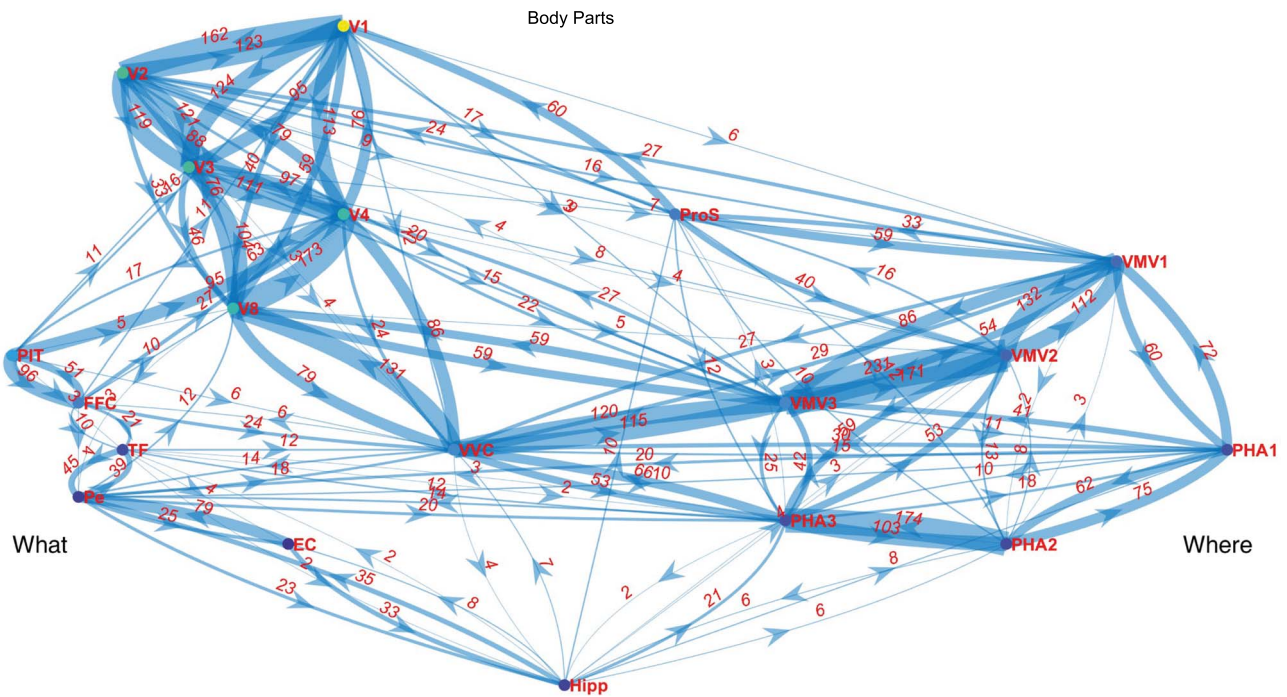


Fig. 6. Visual cortical networks for body parts with 956 HCP participants. The conventions are as in Fig. 3.

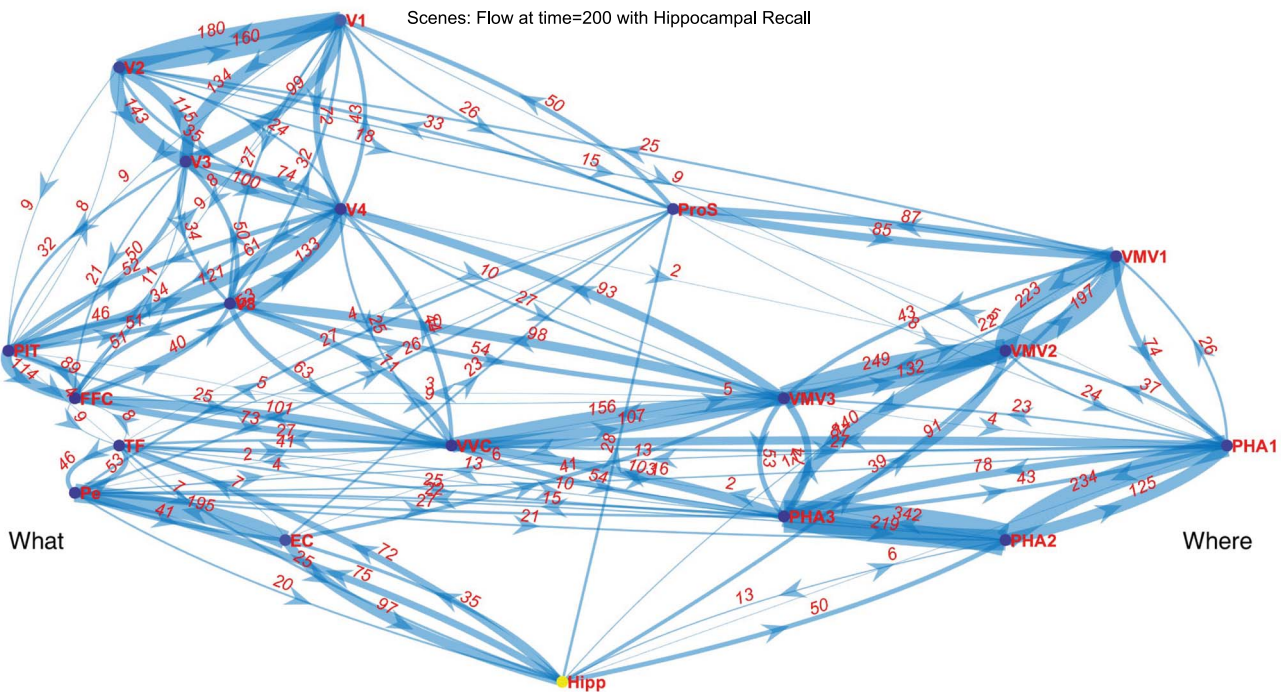


Fig. 7. Reverse flows in the network when a short-term memory operates at the top of the hierarchy. In this case a short-term memory was implemented at the level of the hippocampus by adding an input of 1 at each timestep to the hippocampal node in the network. The flow measured at time = 200. The conventions are as in Fig. 3.

change direction as a function of time since a signal is applied to V1, Fig. 10 shows the flows in the forward direction from V1 to ProStriate cortex (forward), the flow in the backward direction from ProStriate cortex to V1 (backward), and the forward—backward Flow, as a function of the number of timesteps, when the 956 participants were viewing scenes. It is evident that net results of all the effective connectivities between all the 180 nodes in the graph that the net flow of signal reverses between this pair of nodes at about timestep = 165. This clearly demonstrates how

the net direction of signal flow can change after some time in a whole network, and has interesting implications for understanding effective connectivity measurements with the relatively slow timecourse method of fMRI, as shown above in Section Discussion.

Other edges in which the flow changed to be more in the backward direction after 1,000 timesteps include V1 and V2, for which at 40 timesteps the forward vs backward connectivity was 180 vs 73; whereas after 1,000 timesteps it was 180 vs 183 (Figs. 3 and FlowScenes1000).

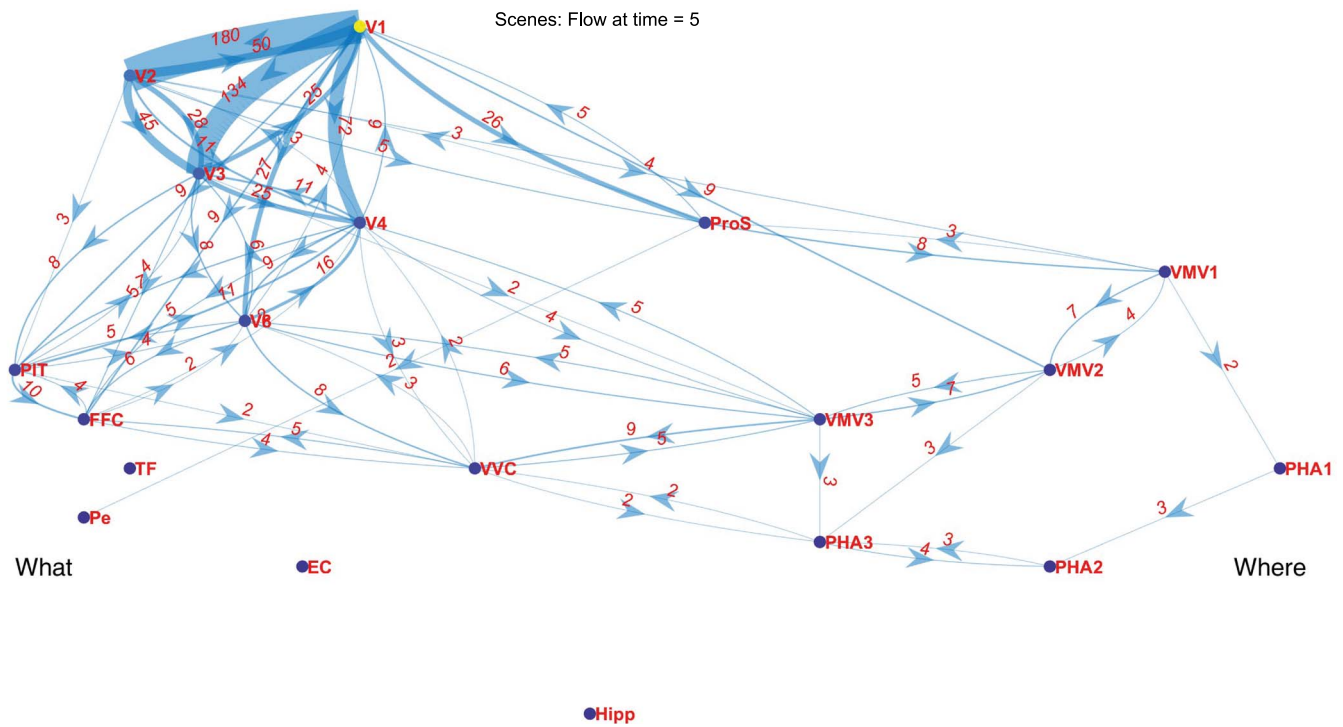


Fig. 8. Visual cortical networks for spatial scenes with 956 HCP participants. The conventions are as in Fig. 3. The flow is now shown at timestep 5. The ventrolateral cortical visual “What” stream is on the left, and the ventromedial cortical visual “Where” stream is on the right.

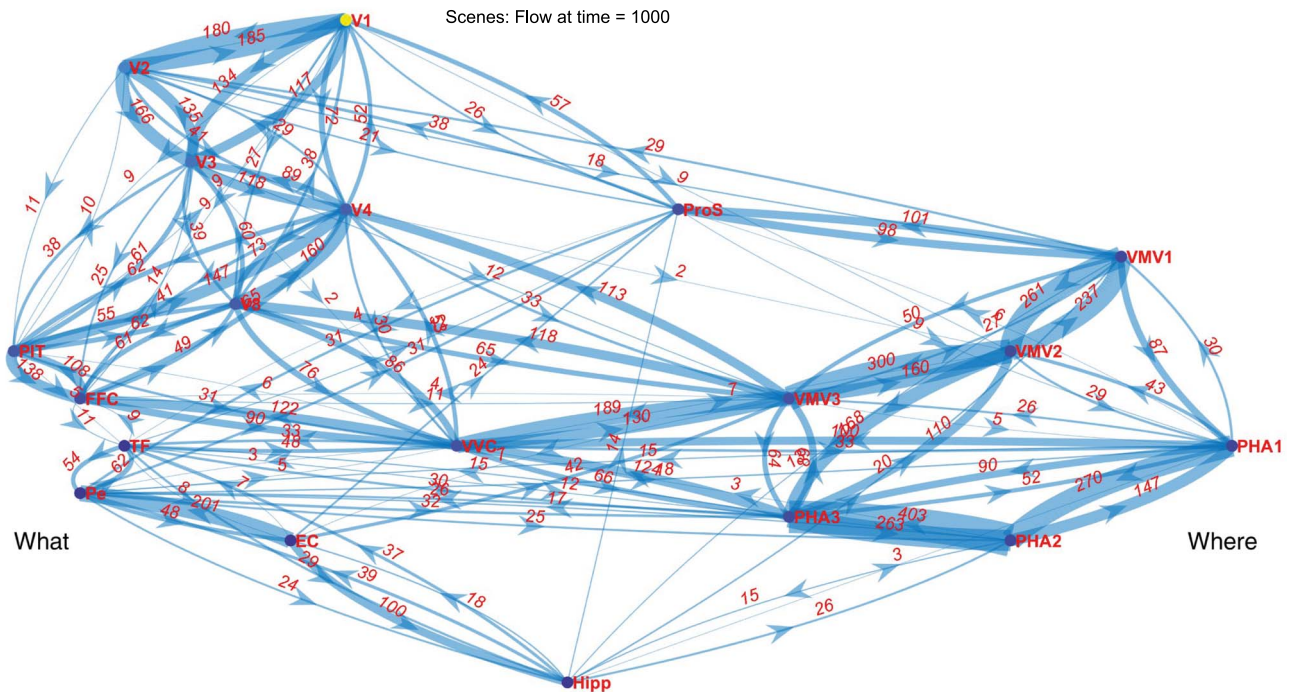


Fig. 9. Visual cortical networks for spatial scenes with 956 HCP participants. The conventions are as in Fig. 3. The flow is now shown at timestep 1,000. The ventrolateral cortical visual “What” stream is on the left, and the ventromedial cortical visual “Where” stream is on the right.

A video to illustrate the development of the flows with the number of timesteps is provided in [Supplementary material](#) as file [RollsVisualCortexDynamicalGraphs.mp4](#), in which the 956 HCP participants were viewing scenes. Use of the pause facility may be helpful when playing this video. This video emphasizes what is in the title of this paper: that we are investigating dynamical graphs, which change as a function of the number of timesteps since a stimulus was applied.

Differences of the flows for different visual stimuli

Statistical tests were performed for the differences in the flows between pairs of cortical regions as described in Section Methods, “Assessment of the differences of the Flows for different visual stimuli”. Examples of these statistical analyses follow, to show that the flows were statistically significantly different when different visual stimuli were being shown. The most useful

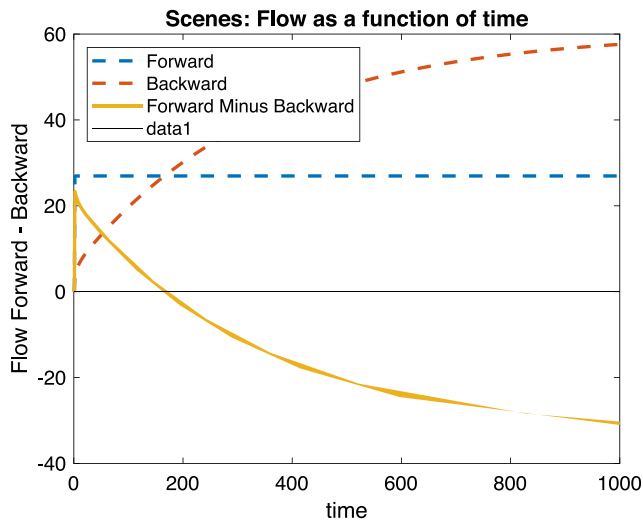


Fig. 10. The flow in the forward direction from V1 to ProStriate cortex (forward), the flow in the backward direction from ProStriate cortex to V1 (backward), and the forward–the backward flow, as a function of the number of timesteps, when the 956 participants were viewing scenes. The flows are multiplied by 1,000 times as in the flow graphs. The horizontal black line shows zero flow, to make it clear when the flow between this pair of nodes reverses direction, at timestep 165.

comparisons are those between scenes and faces, for these are the stimuli that help to define the ventromedial “Where” cortical visual network vs the ventrolateral face/object “What” cortical visual network. Only flows in the direction forward up the hierarchy beyond V4 are reported, as these relate to how information is passed from V4 towards the hippocampal system. The means across the right and left hemispheres are reported. All values are reported that are significant beyond $P \leq 0.01$ after FDR correction and that involve key regions in the ventromedial cortical “Where” stream VMV1-3 and VVC; and that involve a key region in the ventrolateral “Where” stream FFC.

For scenes compared to faces, the flows were greater as follows, where the negative sign for the t values indicates a higher flow to scenes than faces: V4 to VMV2 ($t = -4.2$, $df = 6$, $FDR P = 0.0072$); V4 to VMV3 ($t = -13.3$, $FDR P = 0.0001$); V8 to VMV2 ($t = -5.8$, $FDR P = 0.002$); V8 to VMV3 ($t = -6.7$, $FDR P = 0.0015$); VMV2 to VVC ($t = -3.9$, $FDR P = 0.01$). Thus, the flows in several parts of the ventromedial visual cortical pathway described here for scenes were greater to scenes than to faces for several links in that system, that included all the regions VMV1, VMV2, VMV3, and VVC that are part of this network, as illustrated in Fig. 3.

For faces compared to scenes, the flows were greater as follows, where the positive sign for the t values indicate a higher flow to faces than scenes: V4 to FFC ($t = 4.2$, $df = 6$, $P = 0.006$), FFC to PIT ($t = 6.1$, $FDR P = 0.0072$). Thus, the flows involving the FFC in the ventrolateral visual cortical pathway described here for faces were greater to faces than to scenes for some links in that system, as illustrated in Fig. 4.

It is emphasized that both sets of statistical tests included any links with $P \leq 0.01$ after FDR correction for VMV1, VMV2, VMV3, VVC, and FFC. For the “Where” scene stream, many Flows involving VMV1, VMV2, VMV3, or VVC were significantly higher for scenes than faces, and none for FFC. For the “What” ventrolateral face / object stream, no Flows involving VMV1, VMV2, VMV3, or VVC were significantly higher for faces than scenes, and two involving FFC were significantly higher for faces than scenes. Thus, these statistical analyses provide evidence that

the differences of flow illustrated in for example Figs. 3 and 4 are significantly different. These differences of flow for scenes vs faces are part of the way in which the different dynamical graphs for whole cortical networks related to scenes vs faces are delineated in the approach described here.

Discussion

Key findings are the separation between the “What” ventrolateral visual cortical stream and the “Where” ventromedial cortical stream; the way in which when viewing scenes the flows tended to move more towards the “Where” ventromedial cortical stream and when viewing faces more towards the “What” ventrolateral visual cortical stream; that the flow analyzed over the first 3–30 timesteps can provide evidence about the order in which nodes in the system respond based on the empirically measured effective connectivities; and the finding that the flow can change direction between nodes after long timeperiods.

The graphs that were identified using data from effective connectivity show separate streams (Figs. 2–9). The stream on the left of these figures via FFC, TF, Perirhinal cortex that reaches the hippocampus via the entorhinal cortex can be termed a ventrolateral cortical “What” stream (Rolls 2024b), with information about faces and objects represented in these regions, as shown by an activation study performed in the same 956 participants when they were viewing faces (Rolls et al. 2024b) and using the same HCP-MMP atlas. That identification is supported by the present finding that the flows via this stream were strong when the 956 HCP participants were viewing faces (Fig. 4).

The stream on the right of Figs. 2–9 via the ProStriate cortex, ventromedial cortical regions VMV1–3, and medial parahippocampal regions PHA1–3 that reaches the hippocampus can be termed a ventromedial cortical “Where” stream, with information about scenes represented in these regions, as shown by an activation study performed in the same 956 participants when they were viewing scenes (Rolls et al. 2024b) and using the same HCP-MMP atlas. That identification is supported by the present finding that the flows via this stream were strong when the 956 HCP participants were viewing scenes (Fig. 4).

It is interesting that when tools are being viewed (Fig. 5), the somewhat intermediate region topologically, VVC (see Fig. 1) links together the “What” and “Where” streams by flows between them (and does this more than when faces are being viewed, Fig. 4). Tools also activate the VVC region strongly in these same 956 participants (Rolls et al. 2024b). It was suggested that the activation of VVC by tools may reflect the fact that tools are not only objects, but also have attributes such as where they are and movements that they make, that are likely to be represented in the ventromedial “Where” and visual dorsal stream regions (Rolls et al. 2024b; Rolls 2024b), and the flows in Fig. 5 support this.

It is further interesting that when body parts are being viewed (Fig. 6), there are flows involving “What” stream regions such as FFC, TF, and perirhinal cortex, consistent with the activations (Rolls et al. 2024b). However, there are reverse flows from the hippocampus back into the ventromedial cortical visual stream regions VMV1–3 and VVC, and medial parahippocampal PHA1–3. These reverse flows are associated with no activation of these ventromedial cortical visual stream regions produced by body parts (Rolls et al. 2024b).

The dynamical approach described here is a natural step beyond (static) description and analysis of only a connectivity matrix. Assigning different source (input) nodes by applying to them external stimuli we can highlight the pathways of the

signal precisely from the nodes to which we apply input (V1 in our case). The propagation of signal designed in a natural classical way (eg see related treatment for electrical networks, including random graphs (Doyle and Snell 1984; Bollobás 2013)). Observe that we trace the propagation of signal in time and measure the activity at each node also as a function of time. This allows us to produce a detailed picture of the development of the corresponding directed graphs of the pathways from the source to the destination (hippocampus in our case). We assign to each revealed edge an amount of signal transmitted through it as a function of time. Hence, we end up with a dynamical weighted graph which provides evidence on the relative strength of different possible pathways from one brain region to another for different times.

In the graph analysis, at each timestep the signal moves from a given node to the next nodes with direct connections in the system. The timesteps thus represent the number of successive steps from one node to the connected nodes that have elapsed. This allows analysis of how information may flow through the system, spread from node to node, and how feedback effects from higher nodes in the system can have feedback effects on earlier nodes in the system. Each timestep in the graph-theoretical analysis will not correspond to an exact time in the brain's dynamical system, but an approximate relationship is that it takes ~ 17.5 ms for information to propagate from one cortical region to the next as shown by the time delay from cortical region to cortical region in the ventral visual system. For example, in macaques, the visual response latencies are ~ 30 ms in V1, and then via V2, V4, and posterior inferior temporal cortex are ~ 100 ms in anterior inferior temporal cortex (Rolls 2023a). The times are somewhat longer in the human brain (Rolls et al. 2023e; Rolls 2024c), due in part to the greater connection distances involved. Another type of evidence is that an integrate-and-fire model of the signal flow from V1 to inferior temporal visual cortex shows that with realistic time constants for AMPA, NMDA, and GABA receptors, it takes about 15 ms per stage for the signals to propagate from region to region even allowing for the local recurrent collateral connections within each stage to perform an attractor computation (Panzeri et al. 2001).

It should be noted that as the propagation matrix is derived from the connectivity matrix, the corresponding adjacency matrices (ie without information on the strength of the links) coincide. However, the graphs that describe the flow of signals in the network depend also on the input, ie which nodes I the initial signal is applied to and the strength X of these inputs. Analyzing and visualizing the dynamical flow graphs we highlight the strength of the flow through the edges. It is important to realize that the flow between a pair of nodes is also a function of time and of the input, unlike the strength of connection between these two nodes in a connectivity matrix.

In the computations here we find that the shortest path from V1 to the hippocampus node is via 5–8 nodes. Assuming that a propagation through an edge takes one time step, the graph distance is equivalent to the time for the signal applied to V1 to reach the target at the hippocampus node. Continuing applying the input for a longer time results in the spread of the signal through the network. This leads to the creation of longer paths through different nodes to the destination, and might also build cycles of the flow which contribute to the accumulation of signal. Furthermore, the destination node can also become a node of a cycle which includes even the input node. The cycles in the dynamical graph play an important role of preserving input in certain nodes which could well contribute to memory function.

The findings here are very helpful in going beyond what can be measured with effective connectivity, the strength of the connectivity in each direction between every pair of brain regions. The graph theory based approach described here goes beyond that by considering the direction and strength of the flow between a whole network of cortical regions, so that whole networks connecting distant brain regions can be analyzed, with the flow between different nodes of the network being measured to provide evidence on the relative strength of different possible pathways from one brain region to another. In interpreting these graphs, we should take into account that the flows measured do reflect the effective connectivities, which are based on the functional connectivity and the delayed functional connectivity. Because the effective connectivity could reflect more than direct connections between cortical regions, but could reflect an effect that is felt after a relay in an intermediate cortical area, some of the flows measured extend beyond what might be realized by direct connectivity. For example, in Fig. 4, flow is shown between V1 and V4, but that could reflect in part anatomical connectivity from V1 to V2 or V3 and then to V4. But the flow is very useful, for it provides an indication of the physiological flows of effects between cortical regions, which is helpful for understanding function. It must be remembered that although the net flow of influence can be measured with the methods described here, the actual transmission of information is more forward in a cortical hierarchy, and the backprojections do not send the representation that has reached the top of a hierarchy back to early visual cortical regions (Rolls 2016; 2023a). For example, face neurons are found in the inferior temporal visual cortex but not in V1 (Perrett et al. 1982; Rolls 1984; 2016; 2023a; 2025a). So top-down influences may be useful for top-down attention, and memory recall, but do not simply transmit representations backwards (Rolls 2016; 2023a; Rolls and Treves 2024; Rolls 2025a). Another factor to be taken into account is that the effective connectivity matrix used here was measured with fMRI, and so reflects relatively long-term states that would be present with time delays of 2 s. It will be of interest to measure the flows when the effective connectivity is measured with magnetoencephalography in say 20 ms steps after a stimulus is shown. But despite this point, the graph theory-based analyses of cortical connectivity in humans can provide very useful insight into how different cortical regions interact both in the resting state and when visual stimuli are being delivered in a task.

The finding that the flow can change direction between nodes after long timeperiods is relevant to measuring effective connectivity with fMRI vs magnetoencephalography (Rolls et al. 2023e; Rolls 2024c). With magnetoencephalography, the time delay used to measure the direction of the effective connectivity can be short, for example 20 ms or less, which is close to the propagation time of signal between cortical regions (Panzeri et al. 2001; Rolls 2023a; Rolls et al. 2023e), and the direction of the effective connectivity is away from V1 towards temporal lobe cortical regions (Rolls et al. 2023e; Rolls 2024c), as expected. However, with fMRI, in which the time delay τ for the delayed functional connectivity measure has to be much slower, typically 2,000 ms because of the slow time course of the fMRI BOLD signal, the direction of the effective connectivity appears to be towards V1, and a sign reversal to correct the directionality is applied to the fMRI data (Rolls et al. 2022b; 2022c; 2023a–d, 2023f, 2023g; 2024a). A possible reason for this that has been suggested is that in 2,000 ms the signal produced in V1 by visual stimuli has had plenty of time to reach through the network and for the backprojections between adjacent cortical regions to produce some signal in the backward

direction, which is what is measured with fMRI. That process may be facilitated by short term memory cortical processes in the temporal cortical visual areas and beyond, which is what is illustrated in Fig. 7. But the results shown in Figs. 9 and 10 show that due to the empirically measured effective connectivity effects in both directions between many cortical regions, the net flow can become in the backward direction, due to interactions between cortical regions throughout the network, which includes in this case all 180 regions in the left hemisphere. Thus this graph theory-based approach to understanding the flow of signal in whole connected networks in the brain is helpful in understanding the effective connectivity that is measured empirically with fMRI (Rolls et al. 2022b, 2022c; 2023a–d; 2023f, 2023g; 2024a), and more generally in understanding cortical dynamics across time (Rolls et al. 2023e; Rolls 2024c).

The research described here has wide implications, for here we have new evidence for a human ventromedial visual cortical “Where” network for scenes that is separate from a ventrolateral visual cortical “What” network for faces and objects (Rolls 2023b; Rolls and Treves 2024; Rolls 2024b; 2025a). This advance has as a foundation the discovery of spatial view cells in primates (Cahusac et al. 1989; Rolls 1989; Feigenbaum and Rolls 1991; Rolls and O’Mara 1995; Rolls et al. 1997; Robertson et al. 1998; Rolls et al. 1998; Georges-François et al. 1999; Rolls and Xiang 2005; Rolls et al. 2005; Rolls and Xiang 2006; Rolls 2025a) which is revolutionizing our understanding of hippocampal functioning in primates including humans (Rolls 2023a, b, c; Rolls and Treves 2024). Part of the importance of this revolution is that human episodic memory typically involves remembering where people, objects and rewards or goals are in viewed scenes on particular occasions. We have shown that hippocampal spatial view cells are involved in the rapid association learning and then recall required for this type of episodic memory for objects and their locations in viewed scenes (Rolls et al. 2005; Rolls and Xiang 2006), and rewards and their locations in viewed scenes (Rolls and Xiang 2005). In contrast, in rodents the focus has been on the representation of the place in which the rodent is located, and on path integration between places for navigation that takes into account the head direction and distance moved (O’Keefe and Dostrovsky 1971; O’Keefe 1979; Morris et al. 1982; McNaughton et al. 1983; Burgess and O’Keefe 1996; McNaughton 1996; Samsonovich and McNaughton 1997; McNaughton et al. 2006; Moser et al. 2014; Kropff et al. 2015; Moser et al. 2017; Rolls 2023a; 2025a, 2025b). The rodent findings are consistent with their much poorer visual systems, no fovea, and very wide field of view (De Araujo et al. 2001), and greater reliance on local cues such as touching and exploring local cues with the vibrissae, and olfaction. For primates, spatial view cells are naturally suited to the representations of locations being viewed, and the importance of vision in representing the identity of objects, people, and rewards such as fruit or food, so that the “What,” the “Where,” and the reward value can be associated together where they are combined, in the single attractor network in hippocampal CA3 (Rolls and Treves 2024). This provides enormous adaptive value in finding rewards, people, and objects in the future, by recalling particular memories of where they have been seen (Schobert et al. 2018; Rolls and Treves 2024; Rolls 2024a; Rolls et al. 2024d). The ability of the primate hippocampus to associate viewed locations with reward value (Rolls and Xiang 2005) also has great importance in enabling the emotional or affective value to become a key part of a typical human episodic memory, and in navigation towards goals in viewed locations “out there” (Rolls and Treves 2024; Rolls 2025a). A theory and model for the computations that enable spatial view cells to be

formed along this ventromedial cortical “Where” network to the hippocampus shows how the computations are different from those for faces and objects in the ventrolateral “What” cortical network, highlighting the need for separate cortical networks for the computations for “Where” and “What” representations (Rolls 2025a, 2025c).

The dynamical graph theory approach introduced here has interesting potential for many applications. For example, based on the response properties of neurons in the macaque in the cortex in the superior temporal sulcus (STS) in which neurons respond to combinations of object including face and motion selectivity (Baylis et al. 1985; Perrett 1985; Baylis et al. 1987; Hasselmo et al. 1989a, 1989b; Rolls et al. 2024b) that often have social significance, we proposed (Hasselmo et al. 1989a) that the STS system is a separate system from the ventral cortical visual stream for face and object selectivity, and from the dorsal cortical visual stream, but receives from both of those two streams (Rolls 2024b). This third visual stream to the cortex in the STS has more recently been accepted (Pitcher and Ungerleider 2021). It would be of interest to apply the present graph theory approach to this STS third visual cortical stream, to investigate its connectivity as a network, and how this third network or stream relates to the ventrolateral cortical “What” network and ventromedial cortical “Where” network described here. It would also be of interest to investigate how plasticity in the backprojections in this STS pathway that can influence the ability to perceive face expressions associated with emotions (Borgomaneri 2023) influences this third visual cortical whole network. Another potential application is to understanding the differences between individuals in their whole network connectivity. For example, we have shown that with the same set of visual stimuli described here in the same HCP participants, there are differences between females and males in the activations of visual cortical regions to faces, scenes, body parts, and tools (Zhang et al. 2025). It would be very interesting to use the approach described here to analyze how the whole networks described here differ between females and males.

We emphasize that this approach to analyzing the forward and backward flow of signals in whole networks identified in the approach using directed effective connectivity data for the whole brain is new and unique, as are the results obtained with it, for no other approach in use including dynamic causal modeling (Marreiros et al. 2008; Friston 2009; Stephan 2010; Valdes-Sosa et al. 2011; Friston et al. 2014; Frassle 2017; Razi 2017) can measure effective connectivity across 180 or 360 cortical regions in tasks. Also, Granger causality measures time-related effects between pairs of brain regions (Ge et al. 2012; Shojaie and Fox 2022), whereas for our Hopf effective connectivity the whole matrix of effective connectivities between all nodes in the network that optimally simulates the functional connectivity and delayed functional connectivity across the whole network of nodes (cortical regions) is computed in a whole brain analysis (Deco 2019). In particular, by measuring pairwise effective connectivity over 360 cortical regions when scenes, faces, tools or body parts are being viewed in 956 participants, and by using these new effective connectivity analyses to define whole cortical networks and the flows between the cortical regions in these networks, the present research makes important conceptual contributions to our understanding about what is computed by the human hippocampus for memory and navigation. The research also shows how this is different in key ways from the representations of the place in which the individual is located that provides the present cornerstone for understanding hippocampal system function in rats and mice (Rolls 2023a, 2023b; 2025a), for example by elucidating as

described here a primate including human ventromedial cortical “Where” visual pathway for scenes implemented by spatial view cells (Rolls 2025c).

The networks analyzed here have backprojections from higher regions such as the hippocampus all the way back via multiple cortical regions to early cortical visual processing regions such as V1. Does that fit with deep convolutional network learning approaches to visual information processing in the brain (Yamins and DiCarlo 2016; Zhuang 2021; Celeghin 2023)? There are major issues that arise in those approaches, because so far it is not clear how the local error signals at synapses at every stage of the deep network required for backpropagation of error learning could be generated throughout the network in a biologically plausible way (Rolls 2023a). Another potential problem with this deep learning approach is that if new learning is required when new stimuli become present, the new learning can impair for some time the mappings already learned in the network, and that could be a real problem in a biological system (Song 2024). Another issue is that the cortico-cortical backprojections that connect adjacent stages in the hierarchy are needed for top-down attentional effects (Deco and Rolls 2004; 2005a, b) and memory recall (Rolls and Treves 2024; Rolls et al. 2024d), both of which operate well with associatively modifiable backprojection synapses (Rolls 2023a). An alternative approach to understanding the computations in the visual cortical regions uses biologically plausible competitive networks that utilize local synaptic modification rules, and a short term memory trace to help build transform invariant representations of objects and faces (Rolls 1992; Wallis and Rolls 1997; Wiskott and Sejnowski 2002; Rolls 2012; 2021; 2023a; 2025b).

The conceptual advances provided by the dynamical graph theory approach described here include the following. The approach introduced here allows whole networks of connected brain regions to be investigated, rather than the pairwise node connectivities that are measured by diffusion tractography, functional connectivity, and effective connectivity. This in turn enables analysis of the type described here of whether separate whole cortical networks and pathways or streams are activated by for example viewing scenes compared to faces. Another advance is that the approach described here allows the impact of top-down feedback effects from higher cortical regions, and how these develop over time, to be investigated. For example, the investigation in section “The development of the flows over time” shows that after a long time, the flows will be dominated by top-down flow from the top of the hierarchy to earlier cortical stages, that is, the flows will be in the reverse direction to those of the flow soon after the stimulus is applied. This is very helpful in understanding the effective connectivity measured with the slow neuroimaging method fMRI, in which the effective connectivity can appear to be in the reverse direction of that up the visual hierarchies from early cortical areas that are measured with the fast neuroimaging method of magnetoencephalography (Rolls et al. 2023e; Rolls 2024c). These “reverse flows” are computationally relevant to cognitive functions such as top-down attention (Deco and Rolls 2004; 2005a, 2005b) and memory recall (Rolls and Treves 2024; Rolls et al. 2024d). Another conceptual advance is that the method we introduce here is deterministic, beyond the probabilistic approach sometimes used previously (Fornito et al. 2016; Seguin et al. 2023). Another conceptual advance is that instead of using graph theory to analyze simple features of networks such as the in-degree and out-degree of nodes (Fornito et al. 2016), we show how graph theory can help to understand the dynamical interactions between cortical regions that have effective connectivity between each pair of nodes in

both directions. Another conceptual advance is that because we have been able to measure the effective connectivity in both directions between each pair of 360 cortical regions, we have been able for the first time to investigate as described here some of the bidirectional effects in cortical networks with a relatively large number of nodes in both the ventrolateral “What” and ventromedial “Where” cortical visual pathways to the hippocampal memory system.

In conclusion, the specialized and separate cortical ventromedial scene “Where” network revealed here for what is encoded about locations “out there” in viewed scenes using spatial view cells is fundamental for understanding primate including human hippocampal function in memory and navigation, for the hippocampal system representations in rodents without a fovea and this highly developed visual cortical scene network are primarily about the place where the rodent is located.

Author contributions

Tatyana S. Turova and Edmund T. Rolls developed and wrote the code for the graph flow algorithm together, and Tatyana S. Turova wrote the description in the section: “Model of propagation of signals in a network.” Edmund T. Rolls performed the research with the algorithm, discussed the findings with Tatyana S. Turova, and wrote most of the rest of the paper. Both authors approved the paper for submission. Edmund T. Rolls (Conceptualization, Data curation, Formal analysis, Investigation, Methodology, Project administration, Resources, Software, Validation, Visualization, Writing—original draft, Writing—review & editing), Tatyana S. Turova (Formal analysis, Investigation, Methodology, Writing—review & editing).

Supplementary material

Supplementary material is available at *Cerebral Cortex* online.

Funding

The neuroimaging data were provided by the Human Connectome Project, WU-Minn Consortium (Principal Investigators: David Van Essen and Kamil Ugurbil; 1U54MH091657) funded by the 16 NIH Institutes and Centers that support the NIH Blueprint for Neuroscience Research; and by the McDonnell Center for Systems Neuroscience at Washington University. They and the participants are much appreciated and warmly thanked. Details of the working memory task, and the stimuli used, are available at <https://www.humanconnectome.org/hcp-protocols-ya-task-fmri> and https://db.humanconnectome.org/app/action/ChooseDownloadResources?project=HCP_Resources&resource=Scripts&filePath=HCP_TFMRI_scripts.zip, and are described by Rolls et al. (2024b).

The code for the Hopf effective connectivity was provided by Professor Gustavo Deco, Pompeu Fabra University, and is the same as that used and described previously (Rolls et al. 2023e; Rolls 2024c). Professor Deco is warmly thanked for his great collaboration.

Conflict of interest statement: The authors declare no competing interests.

Data availability

Basic code for the Hopf generative effective connectivity algorithm is available at <https://github.com/decolab/gec>. No new data

were collected in this investigation, and the data analyzed from the Human Connectome Project are available as described above.

References

- Bajaj S, Adhikari BM, Friston KJ, Dhamala M. 2016. Bridging the gap: dynamic causal modeling and granger causality analysis of resting state functional magnetic resonance imaging. *Brain Connect*. 6:652–661. <https://doi.org/10.1089/brain.2016.0422>.
- Barch DM et al. 2013. Function in the human connectome: task-fMRI and individual differences in behavior. *NeuroImage*. 80:169–189. <https://doi.org/10.1016/j.neuroimage.2013.05.033>.
- Baylis GC, Rolls ET, Leonard CM. 1985. Selectivity between faces in the responses of a population of neurons in the cortex in the superior temporal sulcus of the monkey. *Brain Res*. 342:91–102. [https://doi.org/10.1016/0006-8993\(85\)91356-3](https://doi.org/10.1016/0006-8993(85)91356-3).
- Baylis GC, Rolls ET, Leonard CM. 1987. Functional subdivisions of the temporal lobe neocortex. *J Neurosci*. 7:330–342. <https://doi.org/10.1523/JNEUROSCI.07-02-00330.1987>.
- Betzell RF, Faskowitz J, Sporns O. 2023. Living on the edge: network neuroscience beyond nodes. *Trends Cogn Sci*. 27:1068–1084. <https://doi.org/10.1016/j.tics.2023.08.009>.
- Bollobás B. 2013. *Modern graph theory*, Vol. 184.
- Borgomaneri S et al. 2023. Increasing associative plasticity in temporo-occipital back-projections improves visual perception of emotions. *Nat Commun*. 14:5720. <https://doi.org/10.1038/s41467-023-41058-3>.
- Burgess N, O’Keefe J. 1996. Neuronal computations underlying the firing of place cells and their role in navigation. *Hippocampus*. 6:749–762. [https://doi.org/10.1002/\(SICI\)1098-1063\(1996\)6:6<AID-HIPO16>3.0.CO;2-0](https://doi.org/10.1002/(SICI)1098-1063(1996)6:6<AID-HIPO16>3.0.CO;2-0).
- Cahusac PMB, Miyashita Y, Rolls ET. 1989. Responses of hippocampal formation neurons in the monkey related to delayed spatial response and object-place memory tasks. *Behav Brain Res*. 33:229–240. [https://doi.org/10.1016/S0166-4328\(89\)80118-4](https://doi.org/10.1016/S0166-4328(89)80118-4).
- Celeghin A et al. 2023. Convolutional neural networks for vision neuroscience: significance, developments, and outstanding issues. *Front Comput Neurosci*. 17:1153572. <https://doi.org/10.3389/fncom.2023.1153572>.
- De Araujo IET, Rolls ET, Stringer SM. 2001. A view model which accounts for the spatial fields of hippocampal primate spatial view cells and rat place cells. *Hippocampus*. 11:699–706. <https://doi.org/10.1002/hipo.1085>.
- Deco G, Rolls ET. 2004. A neurodynamical cortical model of visual attention and invariant object recognition. *Vis Res*. 44:621–642. <https://doi.org/10.1016/j.visres.2003.09.037>.
- Deco G, Rolls ET. 2005a. Attention, short-term memory, and action selection: a unifying theory. *Prog Neurobiol*. 76:236–256. <https://doi.org/10.1016/j.pneurobio.2005.08.004>.
- Deco G, Rolls ET. 2005b. Neurodynamics of biased competition and co-operation for attention: a model with spiking neurons. *J Neurophysiol*. 94:295–313. <https://doi.org/10.1152/jn.01095.2004>.
- Deco G et al. 2017a. Single or multiple frequency generators in ongoing brain activity: a mechanistic whole-brain model of empirical meg data. *NeuroImage*. 152:538–550. <https://doi.org/10.1016/j.neuroimage.2017.03.023>.
- Deco G, Kringelbach ML, Jirsa VK, Ritter P. 2017b. The dynamics of resting fluctuations in the brain: metastability and its dynamical cortical core. *Sci Rep*. 7:3095. <https://doi.org/10.1038/s41598-017-03073-5>.
- Deco G et al. 2019. Awakening: predicting external stimulation to force transitions between different brain states. *Proc Natl Acad Sci*. 116:18088–18097. <https://doi.org/10.1073/pnas.1905534116>.
- Deen B, Koldewyn K, Kanwisher N, Saxe R. 2015. Functional organization of social perception and cognition in the superior temporal sulcus. *Cereb Cortex*. 25:4596–4609. <https://doi.org/10.1093/cercor/bhv111>.
- Doyle PG, Snell JL. 1984. *Random walks and electric networks*, Vol. 22. American Mathematical Society. <https://doi.org/10.5948/UPO9781614440222>.
- Epstein RA, Baker CI. 2019. Scene perception in the human brain. *Annu Rev Vis Sci*. 5:373–397. <https://doi.org/10.1146/annurev-vision-091718-014809>.
- Epstein RA, Julian JB. 2013. Scene areas in humans and macaques. *Neuron*. 79:615–617. <https://doi.org/10.1016/j.neuron.2013.08.001>.
- Epstein R, Kanwisher N. 1998. A cortical representation of the local visual environment. *Nature*. 392:598–601. <https://doi.org/10.1038/33402>.
- Faskowitz J, Betzel RF, Sporns O. 2022. Edges in brain networks: contributions to models of structure and function. *Netw Neurosci*. 6:1–28. https://doi.org/10.1162/netn_a_00204.
- Feigenbaum JD, Rolls ET. 1991. Allocentric and egocentric spatial information processing in the hippocampal formation of the behaving primate. *Psychobiology*. 19:21–40. <https://doi.org/10.1007/BF03337953>.
- Felleman DJ, Van Essen DC. 1991. Distributed hierarchical processing in the primate cerebral cortex. *Cereb Cortex*. 1:1–47. <https://doi.org/10.1093/cercor/1.1.1>.
- Fornito A, Zalesky A, Bullmore E. 2016. *Fundamentals of brain network analysis*. New York: Academic Press.
- Frassle S et al. 2017. Regression DCM for fMRI. *NeuroImage*. 155:406–421. <https://doi.org/10.1016/j.neuroimage.2017.02.090>.
- Freyer F et al. 2011. Biophysical mechanisms of multistability in resting-state cortical rhythms. *J Neurosci*. 31:6353–6361. <https://doi.org/10.1523/JNEUROSCI.6693-10.2011>.
- Freyer F, Roberts JA, Ritter P, Breakspear M. 2012. A canonical model of multistability and scale-invariance in biological systems. *PLoS Comput Biol*. 8:e1002634. <https://doi.org/10.1371/journal.pcbi.1002634>.
- Friston K. 2009. Causal modelling and brain connectivity in functional magnetic resonance imaging. *PLoS Biol*. 7:e33. <https://doi.org/10.1371/journal.pbio.1000033>.
- Friston KJ, Kahan J, Biswal B, Razi A. 2014. A DCM for resting state fMRI. *NeuroImage*. 94:396–407. <https://doi.org/10.1016/j.neuroimage.2013.12.009>.
- Ge T, Feng J, Grabenhorst F, Rolls ET. 2012. Componential granger causality, and its application to identifying the source and mechanisms of the top-down biased activation that controls attention to affective vs sensory processing. *NeuroImage*. 59:1846–1858. <https://doi.org/10.1016/j.neuroimage.2011.08.047>.
- Georges-François P, Rolls ET, Robertson RG. 1999. Spatial view cells in the primate hippocampus: allocentric view not head direction or eye position or place. *Cereb Cortex*. 9:197–212. <https://doi.org/10.1093/cercor/9.3.197>.
- Gilson M, Moreno-Bote R, Ponce-Alvarez A, Ritter P, Deco G. 2016. Estimation of directed effective connectivity from fMRI functional connectivity hints at asymmetries in the cortical connectome. *PLoS Comput Biol*. 12:e1004762. <https://doi.org/10.1371/journal.pcbi.1004762>.
- Glasser MF et al. 2016a. A multi-modal parcellation of human cerebral cortex. *Nature*. 536:171–178. <https://doi.org/10.1038/nature18933>.
- Glasser MF et al. 2016b. The human connectome project’s neuroimaging approach. *Nat Neurosci*. 19:1175–1187. <https://doi.org/10.1038/nn.4361>.
- Hasselmo ME, Rolls ET, Baylis GC. 1989a. The role of expression and identity in the face-selective responses of neurons in the

- temporal visual cortex of the monkey. *Behav Brain Res.* 32:203–218. [https://doi.org/10.1016/S0166-4328\(89\)80054-3](https://doi.org/10.1016/S0166-4328(89)80054-3).
- Hasselmo ME, Rolls ET, Baylis GC, Nalwa V. 1989b. Object-centred encoding by face-selective neurons in the cortex in the superior temporal sulcus of the monkey. *Exp Brain Res.* 75:417–429. <https://doi.org/10.1007/BF00247948>.
- Heim S et al. 2009. Effective connectivity of the left ba 44, ba 45, and inferior temporal gyrus during lexical and phonological decisions identified with dcm. *Hum Brain Mapp.* 30:392–402. <https://doi.org/10.1002/hbm.20512>.
- Huang CC, Rolls ET, Feng J, Lin CP. 2022. An extended human connectome project multimodal parcellation atlas of the human cortex and subcortical areas. *Brain Struct Funct.* 227:763–778. <https://doi.org/10.1007/s00429-021-02421-6>.
- Kanwisher N, McDermott J, Chun MM. 1997. The fusiform face area: a module in human extrastriate cortex specialized for face perception. *J Neurosci.* 17:4302–4311. <https://doi.org/10.1523/JNEUROSCI.17-11-04302.1997>.
- Kastner S, Chen Q, Jeong SK, Mruczek REB. 2017. A brief comparative review of primate posterior parietal cortex: a novel hypothesis on the human toolmaker. *Neuropsychologia.* 105:123–134. <https://doi.org/10.1016/j.neuropsychologia.2017.01.034>.
- Kosakowski HL et al. 2022. Selective responses to faces, scenes, and bodies in the ventral visual pathway of infants. *Curr Biol.* 32:265–274.e5. <https://doi.org/10.1016/j.cub.2021.10.064>.
- Kringelbach ML, Deco G. 2020. Brain states and transitions: insights from computational neuroscience. *Cell Rep.* 32:108128. <https://doi.org/10.1016/j.celrep.2020.108128>.
- Kringelbach ML, McIntosh AR, Ritter P, Jirsa VK, Deco G. 2015. The rediscovery of slowness: exploring the timing of cognition. *Trends Cogn Sci.* 19:616–628. <https://doi.org/10.1016/j.tics.2015.07.011>.
- Kringelbach ML, Perl YS, Tagliazucchi E, Deco G. 2023. Toward naturalistic neuroscience: mechanisms underlying the flattening of brain hierarchy in movie-watching compared to rest and task. *Sci Adv.* 9:eade6049. <https://doi.org/10.1126/sciadv.ade6049>.
- Kropff E, Carmichael JE, Moser MB, Moser EI. 2015. Speed cells in the medial entorhinal cortex. *Nature.* 523:419–424. <https://doi.org/10.1038/nature14622>.
- Kuznetsov YA. 2013. *Elements of applied bifurcation theory*, Vol. 112. Springer Science and Business Media.
- Maravita A, Romano D. 2018. The parietal lobe and tool use. *Handb Clin Neurol.* 151:481–498. <https://doi.org/10.1016/B978-0-444-63622-5.00025-5>.
- Markov NT et al. 2014. A weighted and directed interareal connectivity matrix for macaque cerebral cortex. *Cereb Cortex.* 24:17–36. <https://doi.org/10.1093/cercor/bhs270>.
- Marreiros AC, Kiebel SJ, Friston KJ. 2008. Dynamic causal modelling for fmri: a two-state model. *NeuroImage.* 39:269–278. <https://doi.org/10.1016/j.neuroimage.2007.08.019>.
- McNaughton BL, Barnes CA, O'Keefe J. 1983. The contributions of position, direction, and velocity to single unit activity in the hippocampus of freely-moving rats. *Exp Brain Res.* 52:41–49. <https://doi.org/10.1007/BF00237147>.
- McNaughton BL et al. 1996. Deciphering the hippocampal polyglot: the hippocampus as a path integration system. *J Exp Biol.* 199:173–185. <https://doi.org/10.1242/jeb.199.1.173>.
- McNaughton BL, Battaglia FP, Jensen O, Moser EI, Moser MB. 2006. Path integration and the neural basis of the 'cognitive map'. *Nat Rev Neurosci.* 7:663–678. <https://doi.org/10.1038/nrn1932>.
- Mishkin M, Ungerleider L, Macko K. 1983. Object vision and spatial vision: two cortical pathways. *Trends Neurosci.* 6:414–417. [https://doi.org/10.1016/0166-2236\(83\)90190-X](https://doi.org/10.1016/0166-2236(83)90190-X).
- Morris RG, Garrud P, Rawlins JN, O'Keefe J. 1982. Place navigation impaired in rats with hippocampal lesions. *Nature.* 297:681–683. <https://doi.org/10.1038/297681a0>.
- Moser EI, Moser MB, Roudi Y. 2014. Network mechanisms of grid cells. *Philos Trans R Soc Lond Ser B Biol Sci.* 369:20120511. <https://doi.org/10.1098/rstb.2012.0511>.
- Moser EI, Moser MB, McNaughton BL. 2017. Spatial representation in the hippocampal formation: a history. *Nat Neurosci.* 20:1448–1464. <https://doi.org/10.1038/nn.4653>.
- O'Keefe J. 1979. A review of the hippocampal place cells. *Prog Neurobiol.* 13:419–439. [https://doi.org/10.1016/0301-0082\(79\)90005-4](https://doi.org/10.1016/0301-0082(79)90005-4).
- O'Keefe J, Dostrovsky J. 1971. The hippocampus as a spatial map: preliminary evidence from unit activity in the freely moving rat. *Brain Res.* 34:171–175. [https://doi.org/10.1016/0006-8993\(71\)90358-1](https://doi.org/10.1016/0006-8993(71)90358-1).
- Orban GA, Sepe A, Bonini L. 2021. Parietal maps of visual signals for bodily action planning. *Brain Struct Funct.* 226:2967–2988. <https://doi.org/10.1007/s00429-021-02378-6>.
- Panzeri S, Rolls ET, Battaglia F, Lavis R. 2001. Speed of feedforward and recurrent processing in multilayer networks of integrate-and-fire neurons. *Network.* 12:423–440. <https://doi.org/10.1080/net.12.4.423.440>.
- Perrett DI, Rolls ET, Caan W. 1982. Visual neurons responsive to faces in the monkey temporal cortex. *Exp Brain Res.* 47:329–342. <https://doi.org/10.1007/BF00239352>.
- Perrett DI et al. 1985. Visual analysis of body movements by neurones in the temporal cortex of the macaque monkey: a preliminary report. *Behav Brain Res.* 16:153–170. [https://doi.org/10.1016/0166-4328\(85\)90089-0](https://doi.org/10.1016/0166-4328(85)90089-0).
- Pitcher D, Ungerleider LG. 2021. Evidence for a third visual pathway specialized for social perception. *Trends Cogn Sci.* 25:100–110. <https://doi.org/10.1016/j.tics.2020.11.006>.
- Pitcher D, Dilks DD, Saxe RR, Triantafyllou C, Kanwisher N. 2011. Differential selectivity for dynamic versus static information in face-selective cortical regions. *NeuroImage.* 56:2356–2363. <https://doi.org/10.1016/j.neuroimage.2011.03.067>.
- Power JD et al. 2011. Functional network organization of the human brain. *Neuron.* 72:665–678. <https://doi.org/10.1016/j.neuron.2011.09.006>.
- Razi A et al. 2017. Large-scale dcms for resting-state fmri. *Netw Neurosci.* 1:222–241. https://doi.org/10.1162/NETN_a_00015.
- Robertson RG, Rolls ET, Georges-François P. 1998. Spatial view cells in the primate hippocampus: effects of removal of view details. *J Neurophysiol.* 79:1145–1156. <https://doi.org/10.1152/jn.1998.79.3.1145>.
- Rolls ET. 1984. Neurons in the cortex of the temporal lobe and in the amygdala of the monkey with responses selective for faces. *Hum Neurobiol.* 3:209–222.
- Rolls ET. 1992. Neurophysiological mechanisms underlying face processing within and beyond the temporal cortical visual areas. *Philos Trans R Soc Lond B.* 335:11–21. <https://doi.org/10.1098/rstb.1992.0002>.
- Rolls ET. 2012. Invariant visual object and face recognition: neural and computational bases, and a model, visnet. *Front Comput Neurosci.* 6:35. <https://doi.org/10.3389/fncom.2012.00035>.
- Rolls ET. 2016. *Cerebral cortex: principles of operation*. Oxford University Press, <https://doi.org/10.1093/acprof:oso/9780198784852.001.0001>.
- Rolls ET. 2021. Learning invariant object and spatial view representations in the brain using slow unsupervised learning. *Front Comput Neurosci.* 15:686239. <https://doi.org/10.3389/fncom.2021.686239>.

- Rolls ET. 2022. The hippocampus, ventromedial prefrontal cortex, and episodic and semantic memory. *Prog Neurobiol.* 217:102334. <https://doi.org/10.1016/j.pneurobio.2022.102334>.
- Rolls ET. 2023a. *Brain computations and connectivity*. Oxford University Press, Open Access. <https://doi.org/10.1093/oso/9780198887911.001.0001>.
- Rolls ET. 2023b. Hippocampal spatial view cells for memory and navigation, and their underlying connectivity in humans. *Hippocampus.* 33:533–572. <https://doi.org/10.1002/hipo.23467>.
- Rolls ET. 2023c. Hippocampal spatial view cells, place cells, and concept cells: view representations. *Hippocampus.* 33:667–687. <https://doi.org/10.1002/hipo.23536>.
- Rolls ET. 2024a. The memory systems of the human brain and generative artificial intelligence. *Heliyon.* 10:e31965. <https://doi.org/10.1016/j.heliyon.2024.e31965>.
- Rolls ET. 2024b. Two what, two where, visual cortical streams in humans. *Neurosci Biobehav Rev.* 160:105650. <https://doi.org/10.1016/j.neubiorev.2024.105650>.
- Rolls ET. 2025a. Hippocampal discoveries: spatial view cells, connectivity, and computations for memory and navigation, in primates including humans. *Hippocampus.* 35:e23666. <https://doi.org/10.1002/hipo.23666>.
- Rolls ET. 2025b. *Neuroscience discoveries*. Oxford University Press.
- Rolls ET. 2025c. A theory and model of scene representations with hippocampal spatial view cells. *Hippocampus.* 35:e70013. <https://doi.org/10.1002/hipo.70013>.
- Rolls ET, O'Mara SM. 1995. View-responsive neurons in the primate hippocampal complex. *Hippocampus.* 5:409–424. <https://doi.org/10.1002/hipo.450050504>.
- Rolls ET, Treves A. 2024. A theory of hippocampal function: new developments. *Prog Neurobiol.* 238:102636. <https://doi.org/10.1016/j.pneurobio.2024.102636>.
- Rolls ET, Xiang J-Z. 2005. Reward-spatial view representations and learning in the hippocampus. *J Neurosci.* 25:6167–6174. <https://doi.org/10.1523/JNEUROSCI.1481-05.2005>.
- Rolls ET, Xiang J-Z. 2006. Spatial view cells in the primate hippocampus, and memory recall. *Rev Neurosci.* 17:175–200. <https://doi.org/10.1515/REVNEURO.2006.17.1-2.175>.
- Rolls ET et al. 1989. Hippocampal neurons in the monkey with activity related to the place in which a stimulus is shown. *J Neurosci.* 9:1835–1845. <https://doi.org/10.1523/JNEUROSCI.09-06-01835.1989>.
- Rolls ET, Robertson RG, Georges-François P. 1997. Spatial view cells in the primate hippocampus. *Eur J Neurosci.* 9:1789–1794. <https://doi.org/10.1111/j.1460-9568.1997.tb01538.x>.
- Rolls ET, Treves A, Robertson RG, Georges-François P, Panzeri S. 1998. Information about spatial view in an ensemble of primate hippocampal cells. *J Neurophysiol.* 79:1797–1813. <https://doi.org/10.1152/jn.1998.79.4.1797>.
- Rolls ET, Xiang J-Z, Franco L. 2005. Object, space and object-space representations in the primate hippocampus. *J Neurophysiol.* 94:833–844. <https://doi.org/10.1152/jn.01063.2004>.
- Rolls ET, Joliot M, Tzourio-Mazoyer N. 2015. Implementation of a new parcellation of the orbitofrontal cortex in the automated anatomical labeling atlas. *NeuroImage.* 122:1–5. <https://doi.org/10.1016/j.neuroimage.2015.07.075>.
- Rolls ET, Huang CC, Lin CP, Feng J, Joliot M. 2020. Automated anatomical labelling atlas 3. *NeuroImage.* 206:116189. <https://doi.org/10.1016/j.neuroimage.2019.116189>.
- Rolls ET, Deco G, Huang CC, Feng J. 2022a. The effective connectivity of the human hippocampal memory system. *Cereb Cortex.* 32:3706–3725. <https://doi.org/10.1093/cercor/bhab442>.
- Rolls ET, Deco G, Huang C-C, Feng J. 2022b. The human language effective connectome. *NeuroImage.* 258:119352. <https://doi.org/10.1016/j.neuroimage.2022.119352>.
- Rolls ET, Deco G, Huang CC, Feng J. 2022c. The human orbitofrontal cortex, vmPFC, and anterior cingulate cortex effective connectome: emotion, memory, and action. *Cereb Cortex.* 33:330–356. <https://doi.org/10.1093/cercor/bhac070>.
- Rolls ET, Deco G, Huang C-C, Feng J. 2023a. Human amygdala compared to orbitofrontal cortex connectivity, and emotion. *Prog Neurobiol.* 220:102385. <https://doi.org/10.1016/j.pneurobio.2022.102385>.
- Rolls ET, Deco G, Huang CC, Feng J. 2023b. The human posterior parietal cortex: effective connectome, and its relation to function. *Cereb Cortex.* 33:3142–3170. <https://doi.org/10.1093/cercor/bhac266>.
- Rolls ET, Deco G, Huang C-C, Feng J. 2023c. Multiple cortical visual streams in humans. *Cereb Cortex.* 33:3319–3349. <https://doi.org/10.1093/cercor/bhac276>.
- Rolls ET, Deco G, Huang CC, Feng J. 2023d. Prefrontal and somatosensory-motor cortex effective connectivity in humans. *Cereb Cortex.* 33:4939–4963. <https://doi.org/10.1093/cercor/bhac391>.
- Rolls ET, Deco G, Zhang Y, Feng J. 2023e. Hierarchical organization of the human ventral visual streams revealed with magnetoencephalography. *Cereb Cortex.* 33:10686–10701. <https://doi.org/10.1093/cercor/bhad318>.
- Rolls ET, Rauschecker JP, Deco G, Huang CC, Feng J. 2023f. Auditory cortical connectivity in humans. *Cereb Cortex.* 33:6207–6227. <https://doi.org/10.1093/cercor/bhac496>.
- Rolls ET, Wirth S, Deco G, Huang C-C, Feng J. 2023g. The human posterior cingulate, retrosplenial and medial parietal cortex effective connectome, and implications for memory and navigation. *Hum Brain Mapp.* 44:629–655. <https://doi.org/10.1002/hbm.26089>.
- Rolls ET, Deco G, Huang CC, Feng J. 2024a. The connectivity of the human frontal pole cortex, and a theory of its involvement in exploit versus explore. *Cereb Cortex.* 34:1–19. <https://doi.org/10.1093/cercor/bhad416>.
- Rolls ET, Feng J, Zhang R. 2024b. Selective activations and functional connectivities to the sight of faces, scenes, body parts and tools in visual and non-visual cortical regions leading to the human hippocampus. *Brain Struct Funct.* 229:1471–1493. <https://doi.org/10.1007/s00429-024-02811-6>.
- Rolls ET et al. 2024c. A ventromedial visual cortical 'where' stream to the human hippocampus for spatial scenes revealed with magnetoencephalography. *Commun Biol.* 7:1047. <https://doi.org/10.1038/s42003-024-06719-z>.
- Rolls ET, Zhang C, Feng J. 2024d. Hippocampal storage and recall of neocortical 'what' - 'where' representations. *Hippocampus.* 34:608–624. <https://doi.org/10.1002/hipo.23636>.
- Rolls ET, Zhang R, Deco G, Vatansever D, Feng J. 2024e. Selective brain activations and connectivities related to the storage and recall of human object-location, reward-location, and word-pair episodic memories. *Hum Brain Mapp.* 45:e70056. <https://doi.org/10.1002/hbm.70056>.
- Rolls ET, Zhang C, Feng J. 2025. Slow semantic learning in the cerebral cortex, and its relation to the hippocampal episodic memory system. *Cereb Cortex.* 35:bhaf107. <https://doi.org/10.1093/cercor/bhaf107>.
- Samsonovich A, McNaughton BL. 1997. Path integration and cognitive mapping in a continuous attractor neural network model. *J Neurosci.* 17:5900–5920. <https://doi.org/10.1523/JNEUROSCI.17-15-05900.1997>.

- Schaefer A et al. 2018. Local-global parcellation of the human cerebral cortex from intrinsic functional connectivity mri. *Cereb Cortex*. 28:3095–3114. <https://doi.org/10.1093/cercor/bhx179>.
- Schobert AK, Corradi-Dell'Acqua C, Fruhholz S, van der Zwaag W, Vuilleumier P. 2018. Functional organization of face processing in the human superior temporal sulcus: a 7t high-resolution fmri study. *Soc Cogn Affect Neurosci*. 13:102–113. <https://doi.org/10.1093/scan/nsx119>.
- Schurz M et al. 2014. Top-down and bottom-up influences on the left ventral occipito-temporal cortex during visual word recognition: an analysis of effective connectivity. *Hum Brain Mapp*. 35:1668–1680. <https://doi.org/10.1002/hbm.22281>.
- Seguin C, Sporns O, Zalesky A. 2023. Brain network communication: concepts, models and applications. *Nat Rev Neurosci*. 24:557–574. <https://doi.org/10.1038/s41583-023-00718-5>.
- Shojaie A, Fox EB. 2022. Granger causality: a review and recent advances. *Annu Rev Stat Appl*. 9:289–319. <https://doi.org/10.1146/annurev-statistics-040120-010930>.
- Smith SM et al. 2013. Resting-state fmri in the human connectome project. *NeuroImage*. 80:144–168. <https://doi.org/10.1016/j.neuroimage.2013.05.039>.
- Song Y et al. 2024. Inferring neural activity before plasticity as a foundation for learning beyond backpropagation. *Nat Neurosci*. 27:348–358. <https://doi.org/10.1038/s41593-023-01514-1>.
- Spiridon M, Fischl B, Kanwisher N. 2006. Location and spatial profile of category-specific regions in human extrastriate cortex. *Hum Brain Mapp*. 27:77–89. <https://doi.org/10.1002/hbm.20169>.
- Sporns O, Tononi G, Kotter R. 2005. The human connectome: a structural description of the human brain. *PLoS Comput Biol*. 1:e42. <https://doi.org/10.1371/journal.pcbi.0010042>.
- Stephan KE, Marshall JC, Penny WD, Friston KJ, Fink GR. 2007a. Inter-hemispheric integration of visual processing during task-driven lateralization. *J Neurosci*. 27:3512–3522. <https://doi.org/10.1523/JNEUROSCI.4766-06.2007>.
- Stephan KE, Weiskopf N, Drysdale PM, Robinson PA, Friston KJ. 2007b. Comparing hemodynamic models with dcm. *NeuroImage*. 38:387–401. <https://doi.org/10.1016/j.neuroimage.2007.07.040>.
- Stephan KE et al. 2010. Ten simple rules for dynamic causal modeling. *NeuroImage*. 49:3099–3109. <https://doi.org/10.1016/j.neuroimage.2009.11.015>.
- Sulpizio V, Galati G, Fattori P, Galletti C, Pitzalis S. 2020. A common neural substrate for processing scenes and egomotion-compatible visual motion. *Brain Struct Funct*. 225:2091–2110. <https://doi.org/10.1007/s00429-020-02112-8>.
- Treves A, Rolls ET. 1994. A computational analysis of the role of the hippocampus in memory. *Hippocampus*. 4:374–391. <https://doi.org/10.1002/hipo.450040319>.
- Tsitsiklis M et al. 2020. Single-neuron representations of spatial targets in humans. *Curr Biol*. 30:245–253.e4. <https://doi.org/10.1016/j.cub.2019.11.048>.
- Urgen BA, Orban GA. 2021. The unique role of parietal cortex in action observation: functional organization for communicative and manipulative actions. *NeuroImage*. 237:118220. <https://doi.org/10.1016/j.neuroimage.2021.118220>.
- Valdes-Sosa PA, Roebroeck A, Daunizeau J, Friston K. 2011. Effective connectivity: influence, causality and biophysical modeling. *NeuroImage*. 58:339–361. <https://doi.org/10.1016/j.neuroimage.2011.03.058>.
- Van Essen DC et al. 2013. The wu-minn human connectome project: an overview. *NeuroImage*. 80:62–79. <https://doi.org/10.1016/j.neuroimage.2013.05.041>.
- Van Essen DC, Glasser MF. 2018. Parcellating cerebral cortex: how invasive animal studies inform noninvasive mapping in humans. *Neuron*. 99:640–663. <https://doi.org/10.1016/j.neuron.2018.07.002>.
- Vul E, Lashkari D, Hsieh PJ, Golland P, Kanwisher N. 2012. Data-driven functional clustering reveals dominance of face, place, and body selectivity in the ventral visual pathway. *J Neurophysiol*. 108:2306–2322. <https://doi.org/10.1152/jn.00354.2011>.
- Wallis G, Rolls ET. 1997. Invariant face and object recognition in the visual system. *Prog Neurobiol*. 51:167–194. [https://doi.org/10.1016/S0301-0082\(96\)00054-8](https://doi.org/10.1016/S0301-0082(96)00054-8).
- Weiner KS, Grill-Spector K. 2013. Neural representations of faces and limbs neighbor in human high-level visual cortex: evidence for a new organization principle. *Psychol Res*. 77:74–97. <https://doi.org/10.1007/s00426-011-0392-x>.
- Weiner KS, Grill-Spector K. 2015. The evolution of face processing networks. *Trends Cogn Sci*. 19:240–241. <https://doi.org/10.1016/j.tics.2015.03.010>.
- Wiskott L, Sejnowski TJ. 2002. Slow feature analysis: unsupervised learning of invariances. *Neural Comput*. 14:715–770. <https://doi.org/10.1162/089976602317318938>.
- Yamins DL, DiCarlo JJ. 2016. Using goal-driven deep learning models to understand sensory cortex. *Nat Neurosci*. 19:356–365. <https://doi.org/10.1038/nn.4244>.
- Zhang R, Rolls ET, Feng J. 2025. Sex differences in activations to the sight of faces, scenes, body parts and tools in visual and non-visual cortical regions leading to the human hippocampus.
- Zhuang C et al. 2021. Unsupervised neural network models of the ventral visual stream. *Proc Natl Acad Sci USA*. 118:e2014196118. <https://doi.org/10.1073/pnas.2014196118>.